Modelling Electrochemical Cell Reactions

Harvey Donnelly | Wellington College Belfast

Comments

Contents

Abstract

In recent decades, research on electrochemical energy storage has focussed primarily on variations of Lithium-Ion batteries, with market leaders such as Panasonic and Samsung investing millions in the technology. However, many experts are concerned due to the finite natural supply of Lithium (1), claiming that even at peak efficiency it will never suffice our impending energy problems. Through digital modelling, I aimed to highlight a select group of cells for further research which show a greater potential of being a viable and cost-efficient alternative energy storage device. By simulating a large group of stable electrochemical cell configurations, I have found that certain cell types, such as Iron Magnesium, can theoretically perform more efficiently than Lithium alternatives while consisting of materials which are relatively abundant and inexpensive.

From the generated models, I have created an extensive catalogue of electrochemical cell configurations from which there are many commercial uses, such as finding the optimal configuration for specific applications. Using them, I have been able to demonstrate how in terms of overall energy efficiency, Iron Electrodes excel, performing consistently well across most areas of assessment. I have also found that cells involving Aluminium and Ferrate electrodes function best in terms of capacity and energy density. Additionally, by use of machine learning through applied neural networks, I have established substantial evidence disproving a direct correlation between a cell's molecular mass and its standard state voltage.

Furthermore, I have also shown from my research how Iron-Ion cell variations are the most efficient when considering high-capacity, grid energy storage and how they could potentially serve as a lower-cost alternative to current Lithium Iron Phosphate devices. Not only do they have a consistently high-power output but they also have impressive energy densities and capacities. However, in terms of mobile electronics, light-weight cells with high energy densities perform best, with far more Lithium electrodes ranking high than with other measures of performance.

Through collaboration with Queen's University Belfast, I have received informed, critical feedback from experts in the field of electrochemistry such as Dr Paul Kavanagh, who I have worked with closely throughout the development of this project. Following his advice, I individually constructed a number of the modelled cell configurations under standard state conditions as to add credibility to the computer-generated results. Upon contrasting the recorded experimental data with the computer-generated models, I am confident that my software and results are generally accurate and credible even though due to technical limitations, I was unable to test certain factors such as operating temperature.

To conclude, by simulating the complex, individual chemical reactions and processes which take place in a battery, I have highlighted many potentially more efficient cell configurations as well as indexing over 300 different electrochemical models from which further studies can cite and use to their advantage. To overcome the world's greatest energy problems, it is pivotal that we develop existing and new battery technologies so that high-capacity energy storage becomes more economical, allowing these kinds of systems to be realistically implemented across the world. In hope of advancing this process, this project aimed to shortlist a number of cells to which more-advanced and specific studies can be based on, exploring each cells feasibility and practical efficiency.

Introduction

Project Overview

Over the last fifty years, it has become increasingly evident that we must find a cost-effective, renewable and non-pollutant source of energy which can accommodate for a fluctuating demand. The rate at which the earth is heating continues to increase due to our stubborn drive to use finite, carbon-based fuels which will inevitably run out in the not-so-distant future. It is my view that this is the greatest threat to modern society. It is for these reasons that I was motivated to study and research the fascinating topic of electrochemical energy storage.

The fact is, we already have a sustainable and non-polluting energy source; solar power. The issue isn't the efficiency of the source itself, it's the inconsistency of power output and the inability to meet an ever-changing demand. The solution? Large-scale electrochemical batteries. In times when the energy requirement is less than the amount being generated, these systems would be able to store any excess energy. The stored electrical potential, could then be used at a later time when the energy demand cannot otherwise be met.

However, this raises the question; why aren't systems like this implemented across the world? The simple answer is that they are too expensive in comparison to less favourable alternatives and the resources used to manufacture them are limited. That is why it is absolutely necessary for us to advance existing and new electrochemical cell technology. In hope of doing so, this project aims to develop a program that models the behaviour of a range of stable cell configurations under a variety of conditions. I aim to verify my model experimentally which will then allow me to confidently highlight any potentially more cost-efficient cell architectures which could spark further investigation into their practicality and feasibility. Furthermore, using intelligent machine learning and custom analysis scripts, I hope to draw various other conclusions on the general behaviour of electrochemical cells so that we can better understand the technology that has become so integrated and essential to our modern way of life.

Hypotheses

(i) "Lithium Cobalt Oxide cells have the highest energy density."

The last decade has seen the rise of the modern smartphone which has given small and dense battery types new relevance. Although lots of research has been done on the subject, one single cell configuration has dominated the market; Lithium Cobalt Oxide cells. An article within the MDPI Journal of Inorganics (2) favoured its involved electrodes in terms of energy density. Based on its sheer popularity and the apparent consensus among the scientific community, I predict that this cell type will perform best when considering optimal energy density.

(ii) "A low combined molecular mass of a cell's electrodes will correlate with having a lower standard voltage."

I predict that the combined molecular mass of a cell's electrodes will correlate negatively with its mean voltage due to an increase in resistance as the transferred ions become more massive. With heavier ions, more energy will be needed to drive an electrical current and so the electrical potential will likely be smaller than that of a lighter cell.

(iii) "Lithium Iron Phosphate cells will be the most efficient at reasonably high operating temperatures (70°C - 100°C)."

As our planet's fossil fuel resources are slowly used up, the electric car industry has been growing at a faster rate than ever before. This recent surge has created new demand for high capacity energy storage. To meet such high capacities, a single cell could never work. Therefore, batteries consisting of a large number of cells are absolutely necessary. Due to this, the cells must be able to work under above average operating temperatures. An article published by the Scientific Journal, Nature Communications (3) found that Lithium Iron Phosphate cells perform the best in terms of overall capacity. Furthermore, major leaders in the industry such as Elon Musk, founder and CEO of Tesla, have invested large sums of money into the development of these types of Lithium Iron cells. It is because of all this, that I imagine the results will support my hypothesis.

(iv) "Moles of transferred electrons will share a positive correlation with capacitance."

As we know from Faraday's law, the moles of transferred electrons reflect an electrode's charge in coulombs. Given charge correlates with capacity, I predict that with a greater number of transferred electrons, there will be a greater capacity.

(v) "A higher operating temperature will result in a higher mean voltage."

Under higher operating temperatures, a cell will ultimately contain more energy in its system than under lower temperatures. I predict that this additional energy will significantly affect the cells open-circuit mean electrical potential, increasing it by a fixed amount for every degree.

Key Terms

Electrochemical Cell

An electrochemical cell either generates electrical energy through chemical processes such as redox reactions or facilitates other electrochemical reactions through the introduction of electricity.

Electrodes

An electrode is defined as being a conductor through which energy enters or leaves an object. When negatively charged, they are referred to as anodes and when positively charged, they are referred to as cathodes. In terms of electrochemistry, an electrode cell is the system in which the oxidation/reduction half-reactions take place.

Redox Reaction

A basic redox reaction involves creating an electrical potential difference between two electrodes through oxidation and reduction. As an anode oxidises, electrons are given out creating a negative charge while the cathode reduces, creating a positive charge. When an electrical current is allowed to flow between the two electrodes, positively charged ions must also flow through a separator/salt bridge in order to balance the charge.

Energy Density

In electrochemistry, energy density refers to the total amount of energy stored in a given mass. In this context, it is typically measured in watthours per gram. A cell with a high energy density will store more power with a smaller mass than one with a lower energy density. It is particularly relevant in the field of mobile electronics where there is an increasing demand for longer battery life from small and light cells.

Fréchet Distance

Named after the French mathematician Maurice Fréchet, this value is a measure of similarity between two curves that takes into account the location and ordering of the points along the curve. By comparing a curve to a straight horizontal line which intercepts at the other plot's median, the value can be used to compare the "flatness" of various curvatures.

Artificial Neural Networks

Inspired by the architecture of our brain, artificial neural networks are complex computer systems which can use machine learning to teach themselves to find relationships between values and executed certain tasks without them being specifically defined. In this project, the technology is used check if complex, otherwise overlooked trends between sets of data exist by searching for a series of mathematical functions which can uniformly connect the inputted variables. If a trend is found, the neural network should be able to predict one variable based on the input of another.

MySQL

MySQL is an open-source database management system based on structured query language. It can be used to store large sets of data in tables in a way that is accessible and readable from a number of different platforms.

Basic Theory

An electrochemical cell, commonly referred to as a battery cell, is a device which facilitates electrochemical processes in which electrons flow from an oxidising negative electrode (anode) to a reducing positive electrode (cathode). This is a known as a Redox reaction although it is frequently described as two half-reactions. An illustration of the electrochemistry in a Lithium Cobalt Oxide cell can be seen in *Figure 1*.

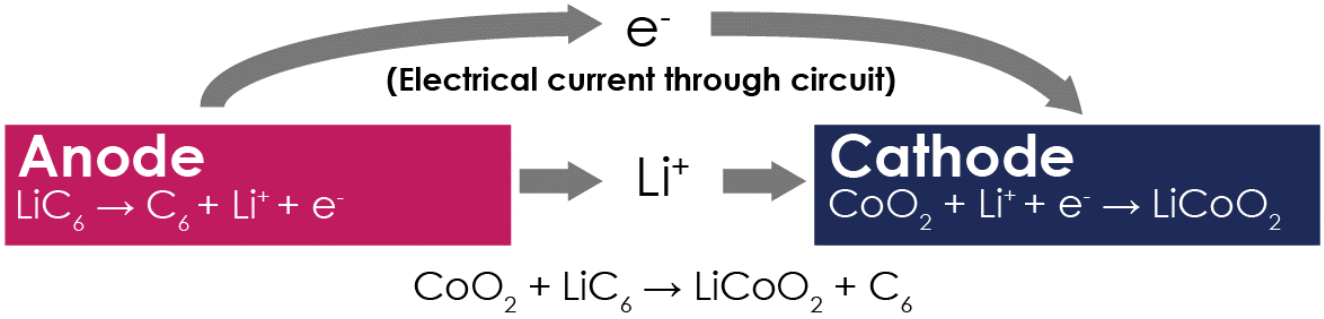

Figure 2 Illustration of the electrochemistry in a Lithium Cobalt Oxide cell

As the Lithiated Graphite anode oxidises, electrons and positive Lithium Ions are produced. As the positive ions flow to the Cathode, the electrons are forced through an electrical circuit before reducing to Lithium Cobalt Oxide. Whenever the reaction is spontaneous, the cell is referred to as Galvanic. In contrast, an Electrolytic cell is one which uses electrical energy to essentially reverse the Galvanic reaction. To summarise, a typical battery is Galvanic while it discharges and Electrolytic whenever it recharges.

To model these processes, the standard reduction potentials of each electrode must be known. These values indicate the tendency for a chemical species to be reduced and are measured in volts at standard conditions. However, they can only be obtained through physical measurements, so I had to gather them from various trusted sources. This along with the atomic mass of each involved element, is all that needs inputted into the system to generate theoretical models of a given cell. By inputting a relatively large repository of electrode data, the software can model every stable cell configuration, allowing for a thorough comparison of cell types.

Data Generation

Electrochemical Cell Modelling System

Beginning as a simple script which modelled a single cell under pre-defined conditions, the Data Generation software has grown to become an incredibly comprehensive and useful tool. Named ECMS (Electrochemical Cell Modelling System), it generates a comprehensive index of redox models under various conditions with the aim of highlighting the most efficient and practical battery cell types for specific situations. Its flexible architecture allows the database to easily scale as more electrode data is inputted, enabling the software to create even larger catalogues in the future with no code modifications.

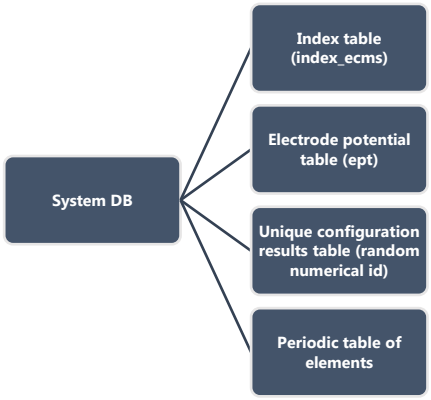

Figure 3 Illustration of the ECMS Database Structure

The python-based program is structured as five primary modules; an executable response module (ECMS), an initialisation module (INIT), an environment configuration module (SEC), a data generation module (DGS), and a chemical syntax decoder module (ECMS_DECODER). The raw data which is produced is stored in a MySQL Database (*Figure 2*) which is hosted on a local server by default (this, among other values, can be easily edited via the application.xml file). Data such as the atomic mass of elements and standard state reduction potentials are vital for many of the calculations and so are stored locally via XML documents.

To summarise, the ecms module is executed first and it runs in an individual thread constantly until all other modules are finished as to feedback what processes are running and to alert if any errors occur. The initialisation module creates all key tables as well as ones which have pre-defined data. Once finished, the SEC module calculates every possible cell configuration and assigns a unique results table and configuration id to each one. Next, the DGS module is imported. This is where various algorithms calculate the data using formula such as the Nernst equation, the results of which are recorded for a wide range of operating temperatures. As these modules are executed, the ECMS_DECODER is regularly called to decode and retrieve information from variables written in the programs proprietary chemical notation syntax.

Proprietary Chemical Notation Syntax

Many of the calculations carried out require the software to understand chemical notation in the same way our brains do. To enable this, I had to create a custom syntax which can be easily read and interpreted by the program (see *Figure 3*).

Syntax	Description
[]	Placed around each object (reactant/product). Every element inside must be combined.
{}	Always contains chemical symbol for an involved element.
{e}	Notation for an electron. It has the same qualities as the {} for elements.
()	First attribute within object brackets. Contains the coefficient of each object.
(())	This attribute follows all parenthesis. It includes the subscript for each element.
((()))	A key attribute, these contain the charge of the surrounding object.
(((())))	The final attribute contains the physical state of the substance.
=	Distinguishes the reactants from the products. Used in place of an arrow.

Figure 4 Proprietary Chemical Notation Syntax

This makes every value clear and accessible, allowing a uniform algorithm to deconstruct each series of notation easily and without any chance of an error occurring. To decode this proprietary syntax, I developed a non-spontaneous module which is regularly called to retrieve certain values from chemical notation. The syntax also aided in analysing the data using Matlab, for the same reasoning.

Calculations and Algorithms

Standard State Voltage

Arguably the most important factor when comparing the efficiency of different cells is their standard electrical potentials. This value indicates the voltage of a cell under typical conditions of 298° Kelvin, air pressure of one atmosphere and concentrations of 1 mole per litre for the reactants/products. However, this value for each electrode can only be obtained by synthesising the cell and manually recording the data; no reasonable equation can be used.

Due to this, the standard reduction potentials for each electrode were gathered from various resources, such as Wikipedia (4) and the MDPI Inorganics Journal (2). This data was manually translated into the before-mentioned proprietary ECMS syntax and stored in an XML document from which it could be easily accessed and interpreted. The oxidation potential was easily calculated by simply multiplying the assigned reduction voltage by negative one. To find the overall standard state voltage of a cell, the program finds the sum of the oxidation and reduction potentials.

Cell Feasibility

A question which frustrated me for many months while working on this project was what defines which electrode will oxidise spontaneously and which will reduce? Originally the software was generating models for both scenarios, however this meant twice the processing load which as I will address later, became a major problem when it came to creating a large amount of models. The only resource (5) I could find which give a clear solution stated that the electrode with the lower standard state voltage will oxidise and the electrode with the higher standard state voltage will reduce. Although I was initially sceptical of this information, I later accepted it after it was supported by my own experimental data (see *Figure 7* on page 11). After successfully implementing it, the processing load halved and the generated results were more streamlined.

Temperature Varying Discharge Curves

Perhaps one of the biggest misconceptions regarding electrochemical cells is that a higher standard state voltage correlates with real-world efficiency for situations requiring a high-power demand. However, this is not the case. Although the magnitude of voltage is certainly a key factor, it is not a dominant one. In most cases the consistency of power output is just as relevant as the median voltage. Given the circuit isn't shorted, the cell's voltage should decrease along a logarithmic curve with the steepest gradients at the beginning and end of its cycle. Nonetheless, the overall steepness can vary greatly depending on which materials are used as electrodes and what temperature the cell is operating in. As many modern electronic devices can only operate within a strict voltage range, having a steeper discharge curve can limit the amount of potentially usable charge.

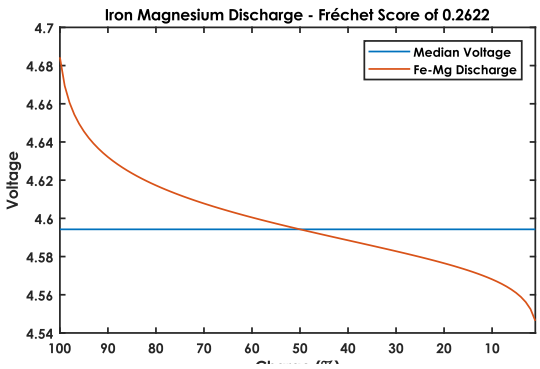

Figure 5 Magnesium Iron Discharge Curve Relative to Median Voltage

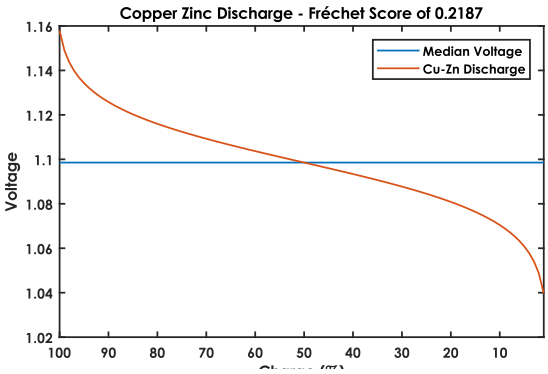

Figure 6 Copper Zinc Discharge Curve relative to Median Voltage

To accurately compare large groups of cells, the Fréchet distance is calculated relative to the median voltage. Note how although the Iron Magnesium cell (*Figure 4*) may have a higher median voltage of about 4.595V relative to 1.098V, the Copper Zinc cell (*Figure 5*) has a more consistent output with a lower Fréchet score (the closer to zero, the better) of 0.2187 in comparison to 0.2622. By assigning a numerical value to the curvature of each cell, I was able

to order each of the configurations by their practical efficiency rather than by more misleading measures such as mean voltage.

These temperature curves were calculated using the Nernst Equation which takes many factors into account to find non-standard state voltages. By looping through this equation, changing certain variables upon each iteration, the program was able to generate accurate voltage curves from various temperatures.

$$E = E^0 - ({}^{RT}/_{nF})\ ln\ Q$$

In this variation of the equation *R* indicates the gas constant of 8.31 Joules per Mole of Kelvin, *F* refers to Faraday's constant of 96,485 Coulombs per Mole of Electrons, *T* is the operating temperature in Kelvin, *n* is the Moles of Electrons transferred, E^0 is the standard state voltage and lastly *Q* represents the reaction Quotient. The reaction quotient is structured as a fraction and the values used to calculate it vary depending on how much it has discharged.

$$Q = \frac{[Products]}{[Reactants]}$$

The Products/Reactants values are calculated by multiplying the activity of each coefficient with the subscript as an index. However, it's not feasible to obtain the activity level of every involved element/compound so their molar concentrations are substituted instead. As the reaction progresses, the concentration of reactants decreases as the concentration of the products increases. When this change is seen graphically as a function of a natural logarithm, we see it forms the basis of the shape of the discharge curve.

All in all, a lot of time and energy was invested into accurately generating varying temperature curves as they are one of the most pivotal factors when considering the overall efficiency of a battery cell. As this algorithm iterates, voltage curves for a range of operating temperatures are inserted into the configuration's unique table from where they can be easily accessed and analysed. By calculating curves for a wide range of temperatures, the software ensures that no potentially revealing configuration goes overlooked and that the optimal cells are easily highlighted for further research.

Capacity

As wind and solar energy industries grow, there is an increasing demand for high-capacity battery storage. It is for this reason that I invested my time to integrate a means of modelling cell capacity into ECMS. The capacity of an electrochemical cell can be calculated using Faraday's law, as seen below.

$$Capacity\ mAh/g = \frac{nF}{m}\ \text{X}\ \frac{5}{18}$$

Firstly, the total charge of the electrode in Coulombs is found by multiplying the moles of electrons transferred by Faraday's constant. To find the charge in C/g, it is divided by the total molecular mass of the two electrodes. Finally, to convert this value into mAh/g, it is multiplied by the constant 0.277 (recurring) or 5/18. This value is then inserted into the ecms_index table where it I assigned to it's appropriate configuration id.

Energy Density

In a world dominated by mobile devices, battery types with high energy densities have been increasingly sought after. To match this growing market, millions of pounds have been invested into developing cell's which can contain the most energy in the smallest mass possible. With this in mind, I believed it to be important to include the energy density for each cell in the ecms_index table. After calculating a cell's capacity in mAh/, the process of finding its energy density is relatively simple. By multiplying this value by the mean voltage, it is possible to find the total amount of Watthours for every gram.

Experimental Verification

Why was it important to record experimental data?

Due to the nature of this project, it would defeat the purpose to manufacture a cell under lab conditions for every modelled configuration and record how it behaves under every operating temperature. However, it would also be bad scientific practice to simply accept the computer-generated results as being accurate without further experimentation. To allow a fair evaluation of the ECMS data, I synthesised a select group of cells, recorded their behaviour and contrasted the results to that generated by the software. Although this did not necessarily prove the accuracy of the computer-generated data, it certainly added credibility.

Materials and Apparatus

Apparatus

- Data Logger/Voltmeter
- Two identical beakers
- Filter Paper
- Resistors (Resistance is dependent on specific cell)
- Conductive Wires
- Safety Goggles

Materials

- Copper Electrode: Copper strip and Copper Sulphate
- Zinc Electrode: Zinc strip and Zinc Sulphate
- Magnesium Electrode: Magnesium strip and Magnesium Sulphate
- Iron Electrode: Iron nail and Iron (ii) Sulphate
- Salt Bridge: Potassium Nitrate
- Solvent: Water

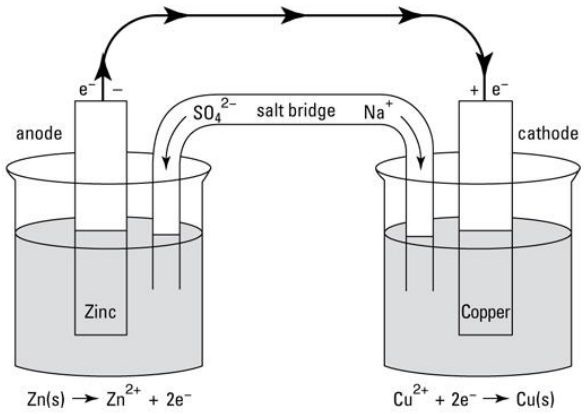

Figure 7 Illustration of Experiment Apparatus and Theory

Method

Firstly, the materials for each of the electrodes were carefully chosen to ensure they would successfully react with each other. After much thought and thorough planning, it was decided that four electrodes could be created with the available resources; Iron/Iron (ii) Sulphate, Zinc/Zinc Sulphate, Copper/Copper Sulphate and Magnesium/Magnesium Sulphate. This meant there was a total of six possible cell configurations which could be tested.

The first configuration to be tested consisted of a Copper Cathode and a Zinc Anode. Two beakers were thoroughly cleaned as to ensure no unwanted substances corrupted the experiment. The base solutions were then prepared in each of them. Both the Copper Sulphate and Zinc Sulphate were sourced in powder form because the larger surface area greatly reduces the time to which they take to dissolve in water.

As planned, both metals were prepared in separate beakers with separate electrolytes. However, for the redox reaction to take place, positive ions must be able to flow freely between the two electrodes. The solution to this was to prepare a salt bridge consisting of filter paper which saturated with a Potassium Nitrate solution (prepared in the same way as the base electrolytes). Before placing the metals in their appropriate electrolytic base solutions, the salt bridge was placed over the two beakers, connecting the two electrodes.

Once a voltmeter was connected via crocodile clips, the open-circuit voltage could be read (see below image). For some of these rudimentary cells, it was approximately equal to the standard state voltage. This is because the voltage is essentially being recorded half-way through its discharge cycle. To record its peak electrical potential, the reaction would have to be manually reversed by driving a current through the cell in reverse. However, the initial energy required to shift the galvanic cell to an electrolytic cell would be too great to even attempt. Nonetheless,

many battery types such as Lithium Cobalt Oxide cells which are typically found in portable electronic devices like smartphones and tablets, do not require nearly as much initial energy to become electrolytic and so are economically viable as a rechargeable form of electrical storage. In the case of the Copper Zinc cell, the recorded voltage with an open circuit was about 1.08V, within the margin of error of the anticipated 1.101V. However, the Magnesium Iron cell appeared to begin its discharge cycle from the very beginning of its curvature (*Figure 7*).

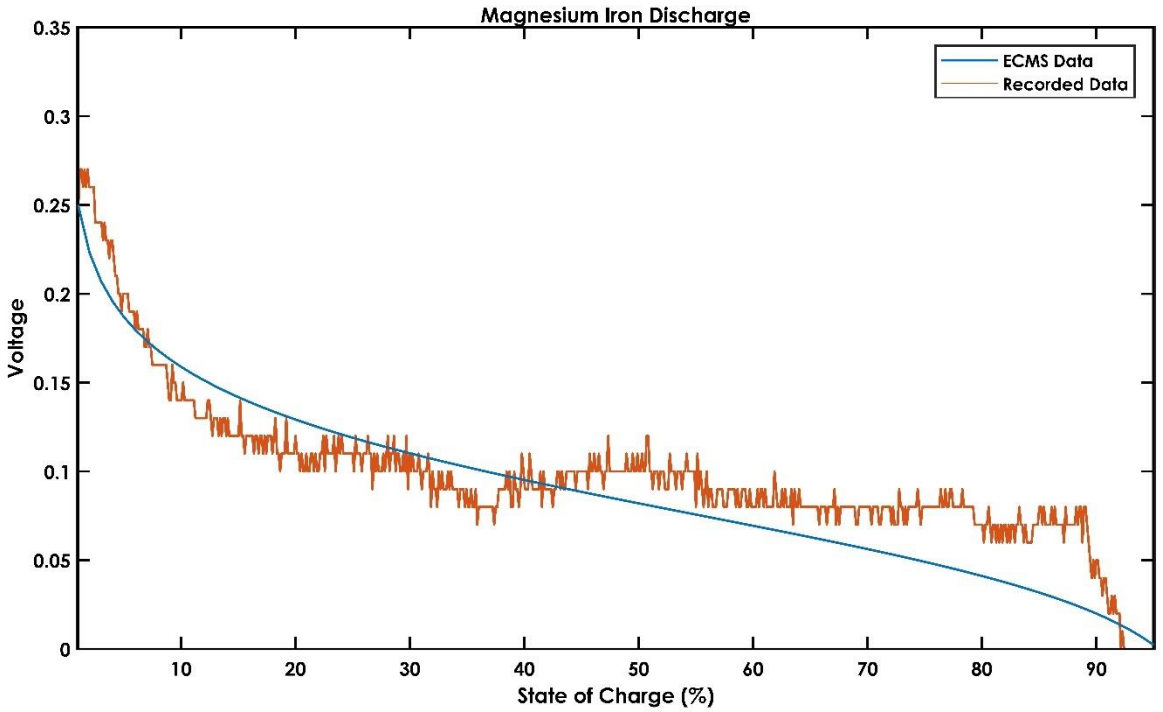

Figure 8 Comparison of experimental data and computer-generated data for the discharge of a Magnesium Iron cell

Unfortunately, the voltage curves calculated by ECMS using the Nernst equation show the theoretical electrical potential of an open circuit as a cell discharges. However, this is impossible to record directly as a cell won't discharge with an open circuit as there must be an electrical current to drain the stored charge. This means a compromise must be made to obtain readable but obtainable results. An appropriate amount of resistance must be used, allowing enough current to flow to discharge the battery but not too little so that the circuit is shorted, and the voltage is not readable (i.e. the voltage equals zero). For the Magnesium Iron cell, a resistance of about 2.8KΩ was used for this. The obtained data can be easily scaled up using Ohm's law for comparison with the computer-generated data (see *Figure 7*).

Conclusion

After repeating this method, a number of times for each planned configuration, I can confidently conclude that the experimental data generally supports the computer-generated data within the fields which I was able to test. With relatively few outliers, most of obtained results stayed within an appropriate margin of error when compared to curves generated by ECMS. Furthermore, I can also surmise that no overlooked factors caused the voltage to drop as the open circuit voltage was recorded for similarly extended periods of time as a control experiment with near-zero discrepancies.

Results Analysis

Methods of Analysis

Machine Learning Through Applied Neural Networks

Thriving at the frontier of modern technology, machine learning is currently aiding scientific research in ways that would have been unthinkable a mere decade ago. With access to a comprehensive database, intelligent neural networks can find complex, otherwise-overlooked relationships between groups of data and then make predictions based on new and unique inputs and/or prove whether there is any correlation at all. Using this revolutionary technology, I aimed to challenge whether certain values are as incalculable and random as is widely accepted. With Matlab's intelligent machine learning and neural network toolboxes, I was able to confidently investigate these kinds of issues and test whether specified trends exist, impervious to human error.

ML Variable Formatting Library

Due to the complex architecture of the ECMS database, formatting variables individually for analysis in Matlab was both time-consuming and inefficient. In hope of resolving this, I developed an m-script library from which I could easily make function calls to generate frequently used variable types such as three-dimensional temperature/discharge matrices and capacity arrays. It was important to do this because I would have otherwise had to manually format and plot variables via scripting in the terminal. Using a personalised library makes analysing and extracting data from such a unique database so much easier and more intuitive.

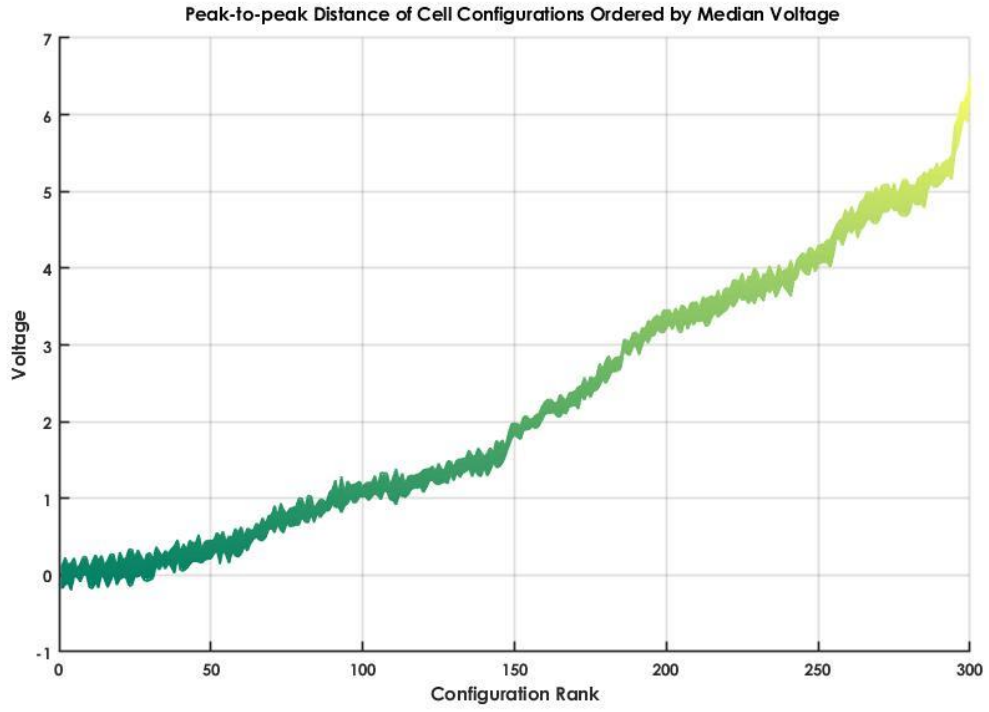

Figure 9 Peak-to-peak Distance of Cell Configurations Ordered by Median Voltage

Figure Generation using Matlab

By using such a reputable and advanced data analysis software, I was able to understand and visualise the results in ways that would have been unimaginable using more conventional programs such as Microsoft Excel. Matlab allowed me to find otherwise unforeseen trends and generate tailored graphs which best demonstrate difficult concepts and findings. Its intelligent toolboxes enabled me to develop neural networks which were used to investigate the absence of correlation between two mathematically unrelated values. Ultimately, without the use of Matlab, I would not be able to accurately express and fully realise the fascinating results hidden within the ECMS database.

Performance due to Discharge Curvature and Operating Temperature

Hypothesis (iii), Hypothesis (v)

Contrary to ***Hypothesis (v)***, the computer-generated results showed that although temperature has a negligible effect on the mean voltage of a cell, it has a more substantial impact on the gradient of its discharge curvature. The data suggests that as its operating temperature increases, the power output becomes more inconsistent. That is to say, at lower temperatures, the plane of usable voltage is greater than at higher operating temperatures. This trend is seemingly uniform for all cell configurations but to varying magnitudes. An inconsistent power output is particularly disadvantageous as in many cases, it means the discharge cycle will be intentionally restricted as to prevent the damage of electronic components.

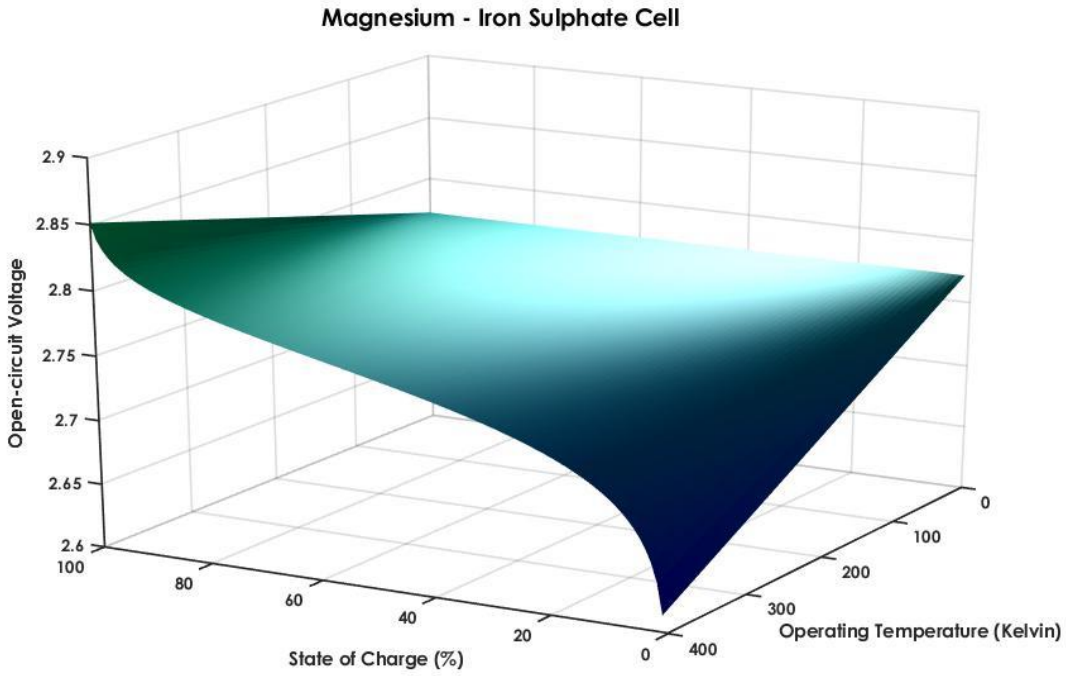

Figure 10 Relationship between voltage curvature and operating temperature for a Magnesium - Iron Sulphate cell

Note *Figure* 9, which demonstrates how the discharge curve of a Magnesium-Iron Sulphate cell changes shape as the operating temperature varies. It is evident from this that a larger portion of the discharge cycle is usable at lower temperatures than at higher temperatures and that the change in curvature is linear (note how the gradient is straight along the temperature axis). Furthermore, these results also make it clear that the curvature at the beginning of the discharge cycle is not necessarily affected by the same magnitude as it is at the end of the discharge cycle.

However, human interpretation can be flawed and easily mislead. With this in mind, it is important to assign a numerical value to each cell's curvature. As I mentioned on page 8, I calculated the Fréchet distances for each cell relative to their median voltage at a given temperature to differentiate between the consistency of power output and accurately compare cell configurations on the basis of voltage uniformity. Upon doing this, the ECMS database revealed that Aluminium Metal cells dominate in terms of energy consistency with six of its configurations present within the top ten. Magnesium, Copper, Beryllium, Zinc and Iron electrodes all feature at least twice, suggesting that energy consistency is more dependent on the characteristics of a single electrode rather than the unique relationship between the two involved electrodes.

Despite this, the Fréchet value does not consider another important factor; voltage (note the lack of definitive correlation in *Figure 10*). Although output consistency is certainly important in most cases, it means nothing if the cell does not have a practical mean voltage. To fairly compare each cell's practical efficiency, I calculated an arbitrary value by dividing the Fréchet distance by the median voltage. The Fréchet-Voltage Score (FV Score for short) is a fair and proportionate way of comparing the overall efficiency of a cell by considering two of the most important factors.

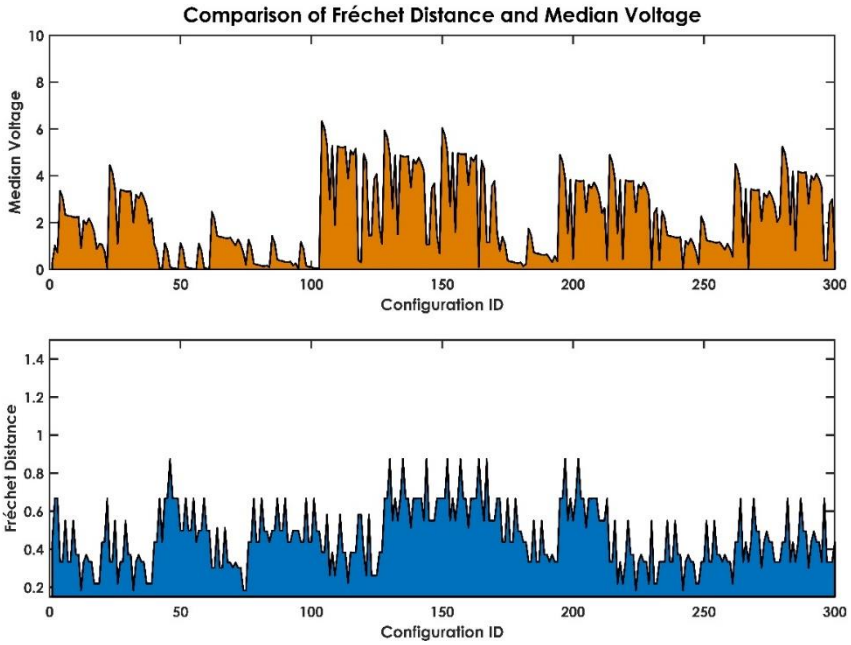

Figure 11 Comparison of Fréchet Distance and Median Voltage

The results produced from this are fascinating (see *Figure 12*). Firstly, Iron and Iron Oxide electrodes dominate in terms of FV score with only one cell containing an Aluminium electrode; a sharp decline from the six found in the Fréchet ranking. The clear superiority in using the FV system over the comparably-primitive Fréchet system is evident in the place-changes between the two lists. All of the Iron/Iron Oxide cells which were only included in the FV rank, were also placed reasonably high on the Fréchet rank. However, many of the highest-ranking cells on the Fréchet system dropped as far as 280 places when judged by FV score. The volatility in placement of these cells

Top Ten Cells by Output Consistency

Cell Configuration	Fréchet Distance	ID
Titanium Aluminium	0.183135699	242
Zinc Aluminium	0.183135699	12
Copper Aluminium	0.183135699	32
Iron Aluminium	0.183135699	224
Aluminium Magnesium	0.183417272	74
Aluminium Beryllium	0.183417272	75
Iron Magnesium	0.218677508	229
Zinc Magnesium	0.218677508	17
Copper Titanium	0.218677508	38
Copper Beryllium	0.218677508	39

Figure 12 Top Ten Cells by Output Consistency

Top Ten Cells by FV Score

Cell Configuration	FV Score	ID
Iron Oxide Magnesium	0.057069	121
Iron Aluminium	0.057305	114
Iron Oxide Strontium	0.060594	104
Iron Oxide Calcium	0.063618	105
Iron Oxide Beryllium	0.064432	125
Iron Oxide Titanium	0.068061	124
Iron Strontium	0.068362	214
Iron Magnesium	0.069582	229
Iron Oxide Lithium	0.07279	108
Iron Calcium	0.072856	215

Figure 13 Top Ten Cells by FV Score

raised concern for their practicality and so following a brief investigation into their discharge curves, I found that most of them have unusably low Voltages. For example, the Titanium Aluminium cell, which shared the highest rank under the Fréchet system, had a theoretical electrical potential of just 0.0302V. In contrast, the Iron Oxide Magnesium cell was ranked a commendable twenty-third when considering output consistency while having a high standard state voltage of 4.572V.

Moreover, as the below-left graph demonstrates, there is an exponential increase in FV Score as the voltage decreases, with a particularly significant impact on points below 1V. Although there is a seemingly negligible reward for increased electrical potential between 1.5V-7V, the small difference in FV Score can still be fairly analysed when outliers are removed. For example, if FV Scores above 1 are not considered, the scale becomes a lot more accurate and a more legitimate comparison can take place. Admittedly, the FV system certainly has its drawbacks, such as significantly losing its accuracy for the worst-performing group of cells with FV Scores of over 1. That being said, this non-linear shift in veracity is negligible when considering the top groups of cells with the FV Scores closest to zero.

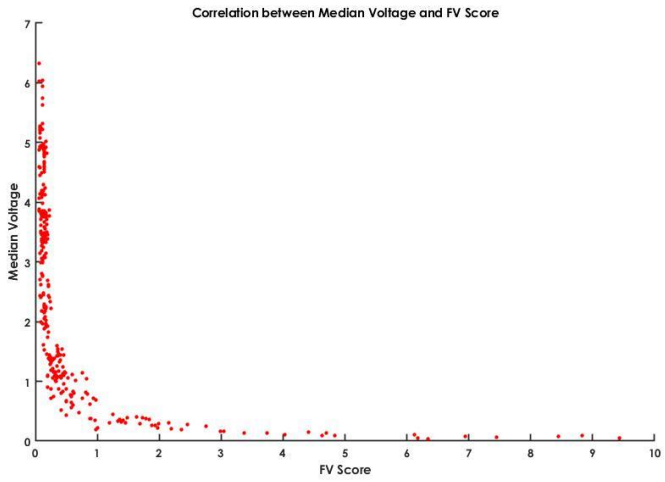

Figure 14 Illustration of the correlation between Median Voltage and FV Score

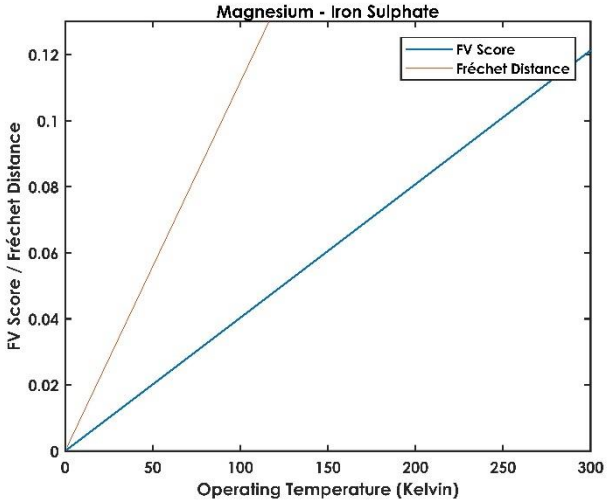

Figure 15 Relationship between Fréchet distance/FV Score and operating temperature for a Magnesium Iron Sulphate cell

Upon analysing the FV Scores at different operating temperatures, I found that the gradient at which they change is positive and linear. Furthermore, each configurations gradient was unique to its own characteristics and was not uniform for all modelled cells. Following an investigation of ***Hypothesis (iii)***, I found the changes in FV rank to be negligible at 398K in retrospect to the already-discussed data at 298K. This applied to Lithium Iron Phosphate which remained at a disappointing 100th place. This suggests that on a performance basis, extreme operating temperatures do not individually affect cells by a significant amplitude and so follow a generally-parallel, collective trend. Furthermore, the Fréchet score shared a similar correlation. Although most cells changed an average of 3 places relative to their rank under standard state conditions, Lithium Iron Phosphate remained at the same, reasonable rank of 29. Ultimately, Lithium Iron Phosphate performs pretty well in terms of output consistency but not in terms of overall efficiency and is far from being considered the optimal cell for above-average operating temperatures. For this title, I would have to also recommend Iron Aluminium for its consistent performance across both the Fréchet system and the FV system at an operating temperature of 398K.

To conclude, from these results, the relationship between output consistency and operating temperature has been made evident. This linear increase in curvature (see above-right graph) suggests cells operating under lower temperatures are more efficient as a larger portion of their discharge cycle is usable. However, attempting to cool a cell from standard state conditions in hope of getting a more efficient discharge curve would not be cost-efficient as the difference at this point on the scale is negligible. Furthermore, the ECMS database has also made it clear that individually, a basic Aluminium electrode performs best in terms of voltage consistency with Iron, Copper, Titanium, Zinc and Beryllium electrodes also exhibiting a high standard under these criteria. However, when it came to comparing the overall efficiency of each cell using FV Scores, Iron and Iron Oxide electrodes dominated. Given its consistency between the FV system and Fréchet system, I believe it's fair to conclude that the Iron Aluminium cell is the most-efficient by compromise of curvature and median open-circuit electrical potential. While remaining one of the most output-consistent cells, it has a high median voltage (3.143V), a high capacity (267.84mAh/g) and a high energy density (841.82Wh/g).

Relationships between Energy Density, Molecular Mass and Capacitance

Hypothesis (i), Hypothesis (v)

In a world dominated by mobile electronics, the energy density and capacity of an electrochemical cell has never been so important. As predicted, my results showed a positive correlation between capacity and energy density (*Figure 15*) and have demonstrated the importance voltage has on Energy Density (notice how the cell with the highest capacity has one of the lowest energy densities). Furthermore, we can see from this data the rate at which the energy density increases is more than that of cell capacity.

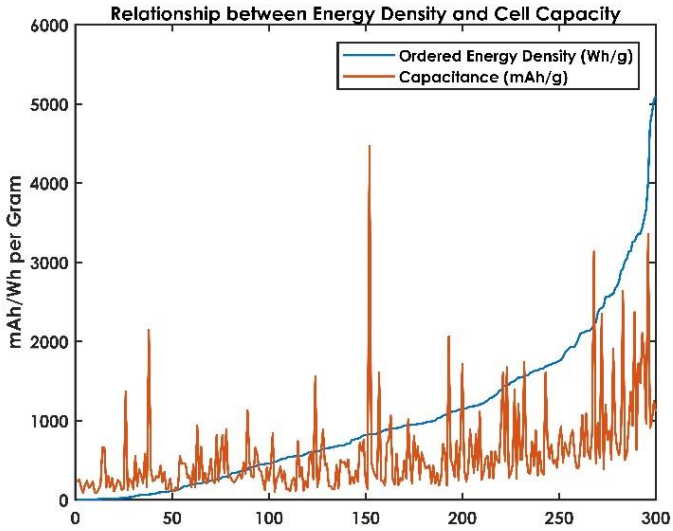

Figure 16 Relationship between energy density and cell capacity

According to Faraday's law, we can also model the correlation between a cells capacitance and the combined molecular mass of its electrodes. As I discussed on page x, cells with a larger combined molecular weight will have a lower capacity. This concept is demonstrated on *Figure 16*. I imagine the negative correlation reflects the increased internal resistance of each cell as the transferred ions become heavier and as a result require more energy to flow.

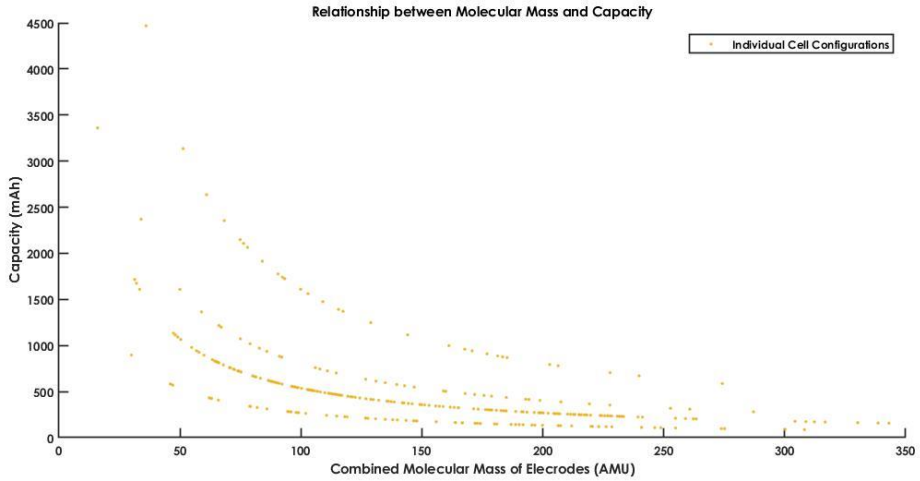

Figure 17 Relationship between molecular mass and capacity

Furthermore, the impact of the number of moles of transferred electrons is clearly visible in how there are four individual trend lines. These lines reflect the small range in values across the ECMS database with the bottom trend line containing all cells with 1 mole of electrons, the second line indicating two, the third line indicating three and lastly the top line indicating six. Supporting ***Hypothesis (iv)***, the relationship is evidently linear as the distances between each line remain fixed to the same ratio. Ultimately, this means a cell with more moles of transferred

electrons will have a significantly higher capacity than a cell with less and will as a result be more resistant to having a higher molecular mass.

Top Ten Cells by Energy Density		
Cell Configuration	**Density (Wh/g)**	**ID**
Ferrate Magnesium	5100.383467	121
Ferrate Beryllium	5050.518648	125
Ferrate Magnesium Sulphate	4879.43903	116
Ferrate Calcium	4744.377329	113
Beryllium Lithium	4008.836785	252
Ferrate Titanium	3672.079359	124
Copper Aluminium	3550.930108	32
Ferrate Lithium	3323.148113	108
Aluminium Lithium	3266.422985	65
Cobalt Aluminium	3258.675686	138

Figure 18 Top Ten Cells by Energy Density

Top Ten Cells by Capacity		
Cell Configuration	**Capacity (mAh/g)**	**ID**
Aluminium Beryllium	4467.692924	75
Beryllium Lithium	3360.017421	252
Aluminium Magnesium	3135.498869	74
Aluminium Lithium	2370.236547	65
Aluminium Magnesium Sulphate	2354.660303	71
Titanium Aluminium	2148.084158	242
Aluminium Calcium	1912.868518	69
Copper Aluminium	1776.353231	32
Zinc Aluminium	1740.892142	12
Magnesium Lithium	1715.514393	186

Figure 19 Top Ten Cells by Capacity

After ordering each cell by energy density (*Figure 17*), one electrode stands out by a surprisingly large magnitude relative to the others. Featured in the top three cells, the Ferrate electrode is clearly the top performer in terms of Energy Density. In direct contradiction with ***Hypothesis (i)***, the Lithium Cobalt Oxide model doesn't even come close to the top performing cells with a comparatively small density of 1071.4 Wh/g and a rank of 91. However, the regular Lithium electrode, among other light-weight metals performed highly with many featuring in the top ten configurations.

Looking at the models ranked by capacity, it becomes clear that light-weight elemental electrodes perform best, with the notable exception of Aluminium Magnesium Sulphate which has six moles of transferred electrons to counteract its additional mass. The Aluminium electrode is the clear top performer although Lithium, Beryllium and Magnesium all feature great capacitance. It can also be noted how the gradient of Capacity is steeper than Density when in order. This indicates that there is a smaller group of electrodes defining the high capacities than there are defining the high energy densities.

All in all, these results have illustrated the direct relationship between capacity and molecular mass and have demonstrated the positive correlation between capacitance and energy density. They have also shown that the moles of transferred electrons share a linear correlation with capacity, allowing more-massive electrodes such as Ferrate and Magnesium Sulphate to outperform some light-weight cells in capacity. The general trend is that electrodes with a high molecular mass and few moles of transferred electrons perform worst in terms of Energy Density and Capacity while light-weight elemental electrodes such as Beryllium, Aluminium and Lithium perform best. I imagine this is because of the increased internal resistance due to heavier ions requiring more energy to flow and cause an electrical current.

Proving a Lack of Correlation between Standard State Voltage and Molecular Mass of Electrodes through Machine Learning

Hypothesis (ii)

With access to a comprehensive database, intelligent neural networks can find complex, otherwise-overlooked relationships between groups of data and then make predictions based on new and unique inputs and/or prove whether there is any correlation at all. Using this revolutionary technology, I aimed to investigate ***Hypothesis (ii)*** and discover whether certain values such as standard state voltage, which are widely accepted as incalculable, show a correlation to other fixed values such as molecular mass.

The first neural network was trained using a total of 40 cells and then tested with a further 15 cells. The training inputs included the median voltage at 298 Kelvin for a random list of cells and the training targets included the molecular mass assigned to each given cell configuration. The performance of a neural network is indicated by the Mean Square Error (MSE). If the MSE is zero, no errors occurred during the validation stage; the closer to zero, the more accurate the trend is. Using Nonlinear input/output Machine Learning techniques, *Network A* performed poorly with a minimum validation MSE of 4.4298, suggesting there isn't a correlation of any kind between the inputs and targets. It's best training details are plotted on *Figure 20*.

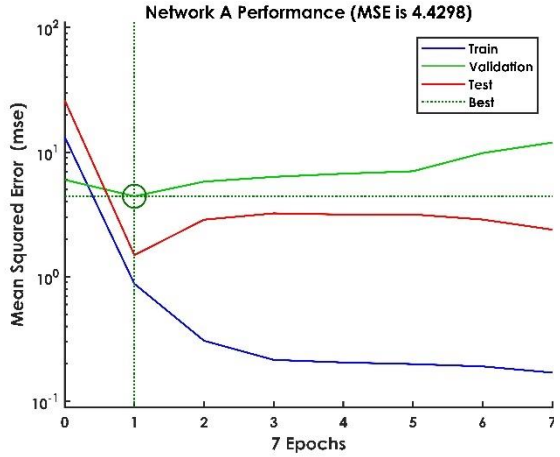

Figure 21 Network A Performance

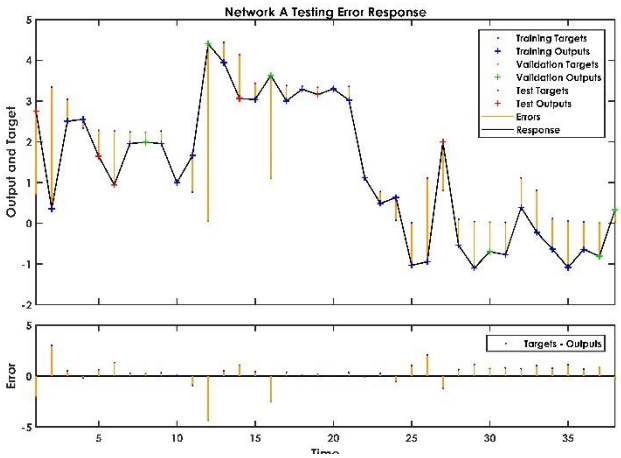

Figure 20 Network A Error Response

The inaccuracy of *Network A* is evident in the Testing Error Response plot (*Figure 19*) where nearly all test outputs are far from their targets. As to ensure the lack of correlation suggested by *Network A* isn't just due to a Machine Learning error, I decided to configure a more complex and tailored neural network, this time using Nonlinear Autoregressive Machine Learning techniques while still using the same 40 inputs and targets.

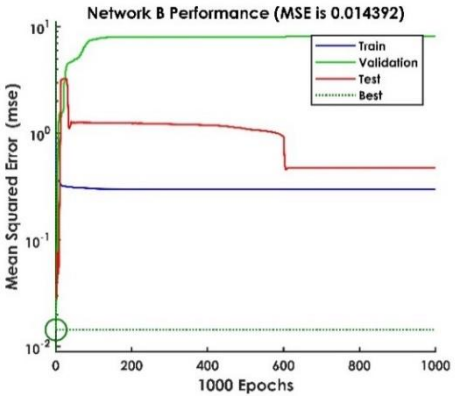

Figure 22 Network B Performance

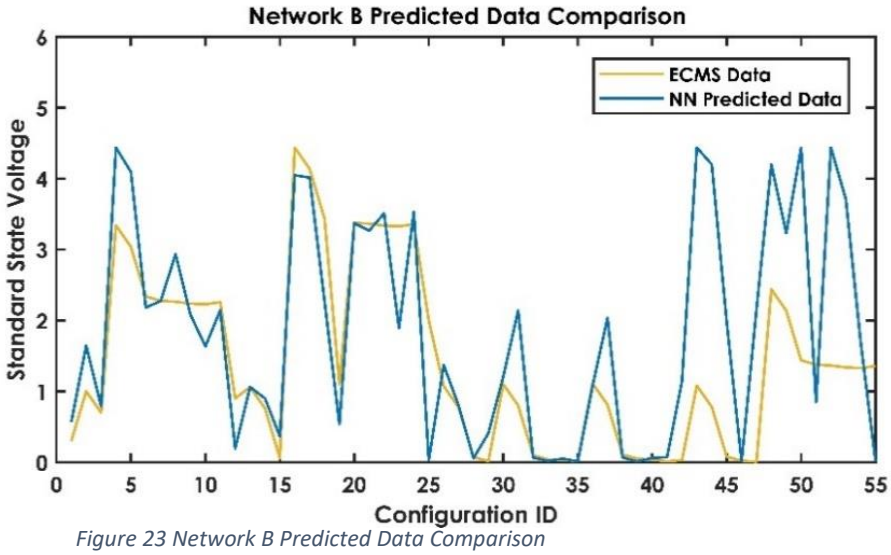

Figure 23 Network B Predicted Data Comparison

After training the new *Network B,* the MSE significantly improved, reaching a very low 0.014392 (*Figure 21)*. Furthermore, when I tested the entire database including the test values, I found the outputted data to be shockingly close (see *Figure 22*).

Perhaps Standard Voltage does correlate with Molecular Mass and ***Hypothesis (ii)*** is wrong? The data from Network B certainly made the topic more complicated. Out of the 15 test configurations (40-55 on *Figure 22*), six were almost perfectly predicted. That being said, the other 60% of test cells were wrongly forecasted by large margins. However, the data did seem to correctly pinpoint which cells would peak above others in terms of voltage, just not to the correct magnitude. All this made it hard to draw any definitive conclusions and so I decided to model more cells using ECMS. With more data used to train the network, the accuracy should improve, given there is a correlation. If not, the MSE should be larger than it was in *Network B*.

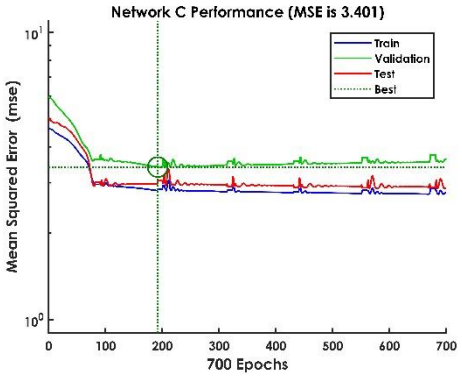

Figure 26 Network C Performance

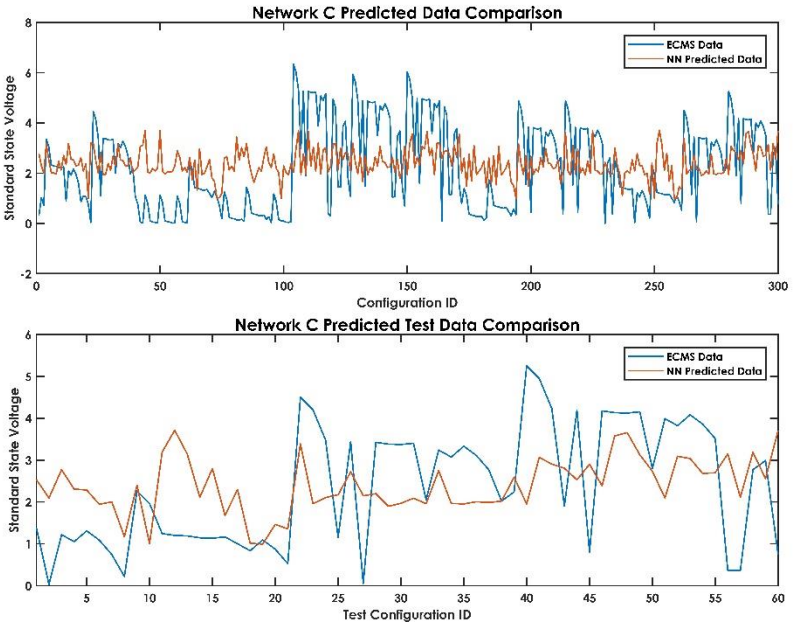

Figure 25 Network C Data Comparisons

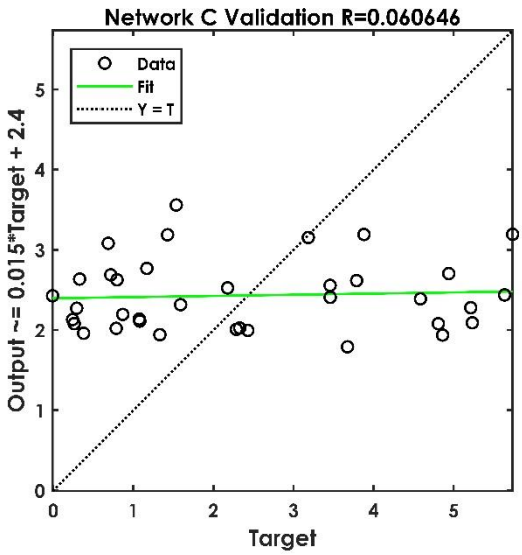

Figure 24 Network C Validation

With 300 models generated, *Network C* was configured in the same way as *Network B* except with more input/target data. With 20% of the configurations put to the side for testing, the network was trained using data for 240 different cells as opposed to the 40 used in *Network B*. The bottom diagram on *Figure 24* demonstrates how when the entire 300 cells are simulated with *Network C,* there is no apparent correlation with the ECMS Data. Furthermore, the top graph on *Figure 24* focuses on the test configurations and how they perform when inputted. With an optimal MSE of 3.401, *Network C* had a Validation score of 0.060646 (*Figures 25 and 26*), indicating the inaccuracy of the networks trend on its own training data (the closer to zero, the less correlation).

By use of the ECMS models, I can conclude with confidence that ***Hypothesis (ii)*** is correct and that there is no correlation between an electrochemical cell's total molecular mass and its standard state voltage. Being impervious to human error, the use of neural networks in the search for a trend between these two sets of variables ensures that if a mathematical relationship existed, it would be highlighted. Although these results do not necessarily challenge the existing consensus, they do provide substantial evidence supporting an otherwise conjectural claim.

Conclusions and Recommendations

By developing scalable electrochemical modelling software, I have been able to assess and evaluate the efficiency of a wide collection of cells under a range of criteria, highlighting a select group to which I can now recommend for further, more-specialised research. From my results, I have not only demonstrated the scope of efficient alternatives to Lithium-Ion variations but have also documented the general behaviour of electrochemical cells along with details for hundreds of specific configurations. Although there are many factors which cannot be practically considered when modelling such a large pool of data, my results have shown clearly that certain configurations show greater potential in terms of capacity, efficiency and energy density than others, streamlining the research and development process and ultimately aiding in the necessary advancement of battery technology.

Firstly, I have illustrated the effect of operating temperature on a cell's efficiency and discharge curvature. My results have shown how a configuration's unique characteristics have a greater effect on output voltage consistency than its environment's temperature and that what little difference it makes is irrelevant as the variation in gradient change across cell configurations is negligible. Ultimately, this means that in terms of overall performance, all cells change with temperature in a nearly uniform fashion, indicating that the most efficient cells at one temperature will be more or less the same at another. It is also important to note how the generated models have shown that at lower operating temperatures, the open-circuit voltage is more consistent throughout the discharge cycle than at higher temperatures. Although the magnitude differs, this trend is seemingly shared by all cell configurations.

The digital models have also highlighted Aluminium electrodes as being best-suited in terms of discharge consistency, although other metal electrodes such as Magnesium, Copper, Beryllium, Zinc and Iron are also top performers. However, this only considers the Fréchet distance of a cells discharge curve relative to a horizontal line intercepting its median. For the fairest comparison, I created my own ranking system involving a value named the FV Score, which acknowledges voltage as well as discharge curvature. Based on my findings, Iron and Iron Oxide electrodes are most efficient, performing with a high yet consistent voltage. However, when examining both measures, one cell stands out; Iron Aluminium. With a consistent power output, high median voltage (3.143V), a high capacity (267.84mAh/g) and a reasonable energy density (841.82Wh/g), it certainly shows a lot of potential in terms of large-scale energy storage.

Moreover, from my results I was able to demonstrate the key relationship between capacity and molecular mass as well as detailing the correlation between capacitance and energy density. The generated models also demonstrated how the number of moles of transferred electrons in a cell's balanced reaction have a linear correlation with capacity, allowing more-massive electrodes such as Ferrate and Magnesium Sulphate to outperform lighter ones in terms of capacity per gram. It is also clear from my results that cell's with a higher molecular mass and fewer moles of electrons will have a low capacity and energy density. After much thought, I credited these trends to increased internal resistance as a result of heavier ions drawing more energy to flow between the cell's electrodes.

Furthermore, using machine learning through applied artificial neural networks, I was able to prove the lack of correlation between molecular mass and standard state voltage. Although the idea is rarely disputed within the scientific community, there is seemingly little/no substantial evidence disproving a relationship between these two pivotal sets of values. After configuring and testing a number of intelligent neural networks with this data as inputs and targets, I can confidently conclude that there is absolutely no correlation between voltage and molecular mass. Some of the developed networks even struggled to find a formula accurately connecting the training data, let alone the validation and test data. Collectively, the models were again able to provide new insight into electrochemical cell technology in ways that would not have otherwise been possible.

In order to verify the generated models, I synthesised a number of cell configurations and recorded their voltage as they discharged. Upon contrasting the appropriately formatted results to the predicted information, I found that generally, the experimental data supported the models. That being said, only these specific variables were able to be recorded under fixed standard state conditions due to technical limitations. Ideally, this and other cell characteristics should be tested under a range of operating temperatures as to validate all aspects of the modelling system, adding

further credibility to the generated data. After collaborating with Queen's University lecturer in electrochemistry, Dr Kavanagh, it was initially planned to conduct such experiments using the necessary materials and equipment from the University's Chemical Engineering Department. However, following weeks of discussion we decided that it would be too difficult and complicated to organise such experiments during college assessment periods and so the arrangement never worked out. All things considered, there is already enough experimental data gathered to ensure the level of validity needed for the software to function well and realise its ultimate purpose.

That being said, there are still ways to improve the accuracy and continuity of the modelling system. When calculating the reaction quotient (a vital component of the Nernst equation), concentrations of the reactants/products are used to substitute the ionic activity values of each involved element. Depending on these exact values, the accuracy of a given cell model will vary. I intend to address this issue in the near future as well as integrating support for modelling cells specifically in acidic and basic solutions. Additionally, I aim to reduce execution load of the electrochemical modelling program as to allow for the practical generation of even more models.

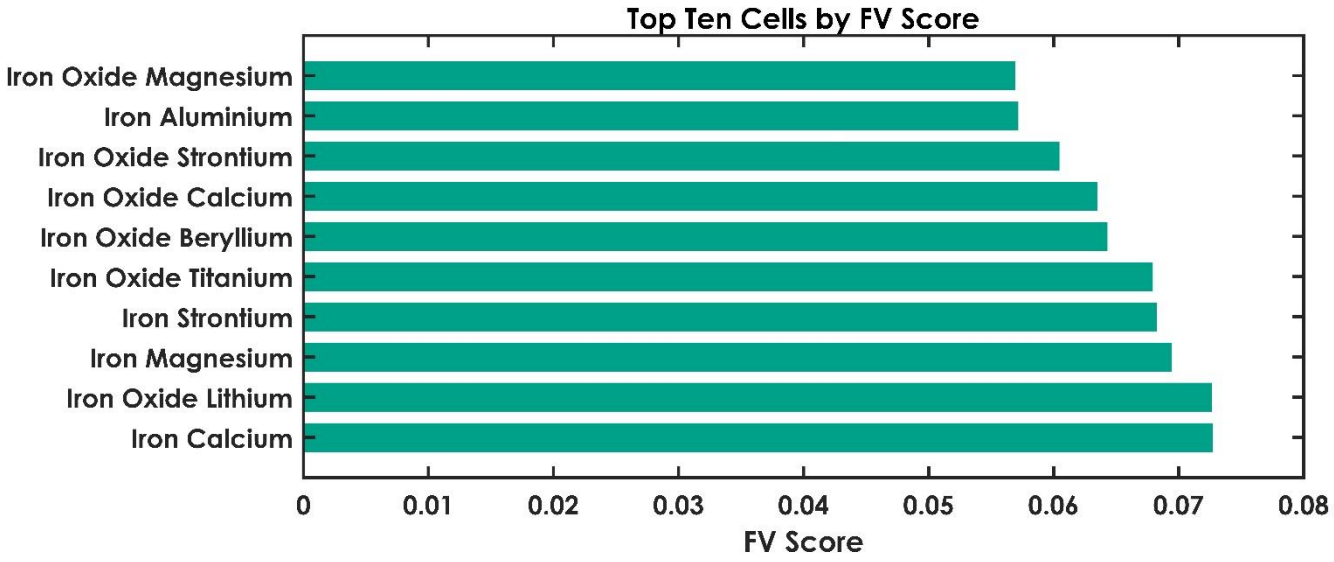

Figure 27 Bar chart showing Top Ten Cells by FV Score

In closing, by pursuing new and innovative cell technologies, pressing issues such as climate change and our reliance on finite energy sources can be realistically addressed in the coming decades. Ultimately, the aim of this project is to advance the rate at which this research and development is carried out by highlighting plausible cell configurations which perform highly when modelled under certain criteria such as capacity, energy density, output consistency and mean voltage. The developed modelling technology can be used as a useful tool for researchers and businesses for a variety of applications and the models generated can be cited as an index of electrochemical cells and their behaviour. All in all, I have found that in terms of large-scale, grid energy storage, cells with variations of Iron electrodes (e.g. Iron, Iron Oxide, Ferrate $^{etc.}$) perform best while consisting of abundant and comparably inexpensive materials (*Figure 26*). Specifically, Iron Aluminium and Iron Magnesium configurations have been consistent performers across all measures although their above-average mass prevents them from being viable alternatives to Lithium-Ion cells in terms of mobile electronic devices. Although for these scenarios, my data has shown that variations of Lithium and Beryllium cells are best suited, most future investment will likely be found in the area of high-capacity renewable energy storage to which my models predict Iron-Ion battery technology will excel in. Based on my models and results, I have decided to advocate for further investment in Iron-Ion storage and recommend that these various configurations be studied and tested for their practicality and feasibility.

Acknowledgements

First and foremost, I would like to thank my Physics teacher, David Cardwell, for his guidance and support. His commitment and dedication remained unrivalled during the development of the project and I am grateful for all that he invested. I am also grateful to my father, Ronan Donnelly, for his support and encouragement through these stressful times and I owe much of the completion of this project to him. I also appreciate all the help and support provided by other friends and members of my family who backed and encouraged me all while I was busy working on this.

Furthermore, I am grateful to Dr Paul Kavanagh of Queen's University Belfast to whom I regularly collaborated with for his expert feedback and advice and for his continued dedication. His sacrifice and guidance does not go under-appreciated. I would also like to acknowledge Professor Peter Allen from the University of Idaho for his experienced and valued consultation. Lastly, I would like to thank other teachers and members of staff at my college for their devoted support and encouragement as I developed this project.

References

Table of Figures

Bibliography

1. **West, Karl.** Carmakers' electric dreams depend on supplies of rare minerals. *The Guardian.* [Online] 2017. https://www.theguardian.com/environment/2017/jul/29/electric-cars-battery-manufacturing-cobalt-mining.

2. **Julien, Christian, et al.** Comparative Issues of Cathode Materials for Li-Ion Batteries. *MDPI Inorganics.* [Online] 2014. http://www.mdpi.com/2304-6740/2/1/132.

3. **Hu, Lung-Hao, et al.** Graphene-modified LiFePO4 cathode for lithium ion battery beyond theoretical capacity. *Nature Communications.* [Online] 2013. https://www.nature.com/articles/ncomms2705.

4. **Wikipedia.** Standard Electrode Potentials Data Page. [Online] https://en.wikipedia.org/wiki/Standard_electrode_potential_(data_page).

5. **ChemGuide.** Making predictions using redox potentials. [Online] https://www.chemguide.co.uk/physical/redoxeqia/predict.html.

6. **Nowak, Pawel and Koziol, Barbara.** On the rest potential of Pyrite Electrode in Oxygen-free solutions of Iron(II) Sulphate. *Polish Academy of Sciences.* [Online] 2002. http://www.minproc.pwr.wroc.pl/journal/pdf/2002/s77-88.pdf.

7. **Barpanda, Prabeer, et al.** A 3.8-V earth-abundant sodium battery electrode. *Nature Communications.* [Online] 2014. https://www.nature.com/articles/ncomms5358.

8. **Chanrasekran, Rajeswari.** Modelling of Electrochemical Energy Storage and Energy Conversion Devices. *Georgia Institute of Technology.* [Online] 2010. https://smartech.gatech.edu/bitstream/handle/1853/37292/chandrasekaran_rajeswari_201012_phd.pdf.

9. **Chueh, William.** Electrochemical & Thermochemical Behavior of CeO2-δ. *California Institute of Technology.* [Online] 2011. https://thesis.library.caltech.edu/6170/2/ChuehThesis.pdf.

10. **Cohn, Adam, et al.** Anode-Free Sodium Battery through in Situ plating of Sodium Metal. *Nano Letters.* [Online] 2017. http://pubs.acs.org/doi/abs/10.1021/acs.nanolett.6b05174.

11. **Nitta, Naoki, et al.** Li-ion battery materials; present and future. *ScienceDirect.* [Online] 2014. https://www.sciencedirect.com/science/article/pii/S1369702114004118.

Model Index

SSVP*: *Standard State Voltage* ***TCPG*:*** *Capacity in mAh/g* ***TEDPG*:*** *Energy Density in Wh/g*
CMW*: *Combined Molecular Mass of Electrodes* ***MTE*:*** *Moles of Transferred Electrons*

Please note, the Model Index does not include the Redox Syntax for each cell due to size restrictions.

ID	Cathode	Anode	FV Score	Fréchet Score	SSVP*	TCPG*	TEDPG*	CMW*	MTE*
1	Calcium	Strontium	1.455465631	0.437355015	0.301	209.8818	63.17441	127.698	1
2	Praseodymium	Strontium	0.655610141	0.667268675	1.001	117.2789	117.3962	228.5277	1
3	Praseodymium	Calcium	0.930921816	0.667268675	0.7	148.0862	103.6603	180.9857	1
4	Zinc	Strontium	0.099663998	0.333634338	3.3392	350.3233	1169.799	153.01	2
5	Zinc	Calcium	0.109510695	0.333634338	3.0382	508.2391	1544.132	105.468	2
6	Zinc	Praseodymium	0.235919393	0.549407098	2.3382	259.8331	607.5417	206.2977	2
7	Zinc	Lithium	0.145902654	0.333634338	2.2783	741.0787	1688.4	72.331	2
8	Zinc	Caesium	0.146807888	0.333634338	2.2642	270.3187	612.0557	198.2954	2
9	Zinc	Erbium	0.246504474	0.549407098	2.2382	230.4017	515.6852	232.65	2
10	Zinc	Barium Hydroxide	0.167208955	0.371086853	2.2282	243.9522	543.5742	219.7273	2
11	Zinc	Calcium Hydroxide	0.164978809	0.371086853	2.2582	437.6633	988.3313	122.4753	2
12	Zinc	Aluminium	0.204150124	0.183135699	0.9002	1740.892	1567.151	92.37154	6
13	Zinc	Lithiated Graphite	0.15989443	0.333634338	2.0782	371.2194	771.4681	144.397	2
14	Zinc	Magnesium Hydroxide	0.193344881	0.371086853	1.9282	502.3598	968.6501	106.7023	2
15	Zinc	Potassium	0.153212556	0.333634338	2.1692	513.0044	1112.809	104.4883	2
16	Zinc	Sodium	0.170518149	0.333634338	1.9482	606.5072	1181.597	88.37977	2
17	Zinc	Magnesium	0.135829117	0.218677508	1.6102	597.6137	962.2776	89.695	2
18	Zinc	Titanium	0.251948363	0.218677508	0.8682	473.2318	410.8598	113.27	2
19	Zinc	Beryllium	0.20155617	0.218677508	1.0852	720.4488	781.8311	74.40218	2
20	Lithium	Strontium	0.412446748	0.437355015	1.0609	283.4306	300.6915	94.561	1
21	Lithium	Calcium	0.575928265	0.437355015	0.7599	570.0139	433.1535	47.019	1
22	Lithium	Praseodymium	16.00309732	0.665596064	0.0599	181.2764	10.85846	147.8487	1
23	Copper	Strontium	0.075034856	0.333634338	4.438	354.5967	1573.7	151.166	2
24	Copper	Calcium	0.080483194	0.333634338	4.137	517.2833	2140.001	103.624	2
25	Copper	Praseodymium	0.160289545	0.549407098	3.437	262.1765	901.1008	204.4537	2
26	Copper	Zinc	0.199060904	0.218677508	1.0988	415.7331	456.8075	128.936	2
27	Copper	Lithium	0.098548276	0.333634338	3.3771	760.4659	2568.17	70.487	2
28	Copper	Caesium	0.09896043	0.333634338	3.363	272.8561	917.6151	196.4514	2
29	Copper	Erbium	0.165106529	0.549407098	3.337	232.2425	774.9932	230.806	2
30	Copper	Barium Hydroxide	0.111837148	0.371086853	3.327	246.0168	818.4979	217.8833	2
31	Copper	Calcium Hydroxide	0.110835053	0.371086853	3.357	444.3535	1491.695	120.6313	2
32	Copper	Aluminium	0.091757611	0.183135699	1.999	1776.353	3550.93	90.52754	6
33	Copper	Lithiated Graphite	0.104738884	0.333634338	3.177	376.0213	1194.62	142.553	2
34	Copper	Magnesium Hydroxide	0.122953792	0.371086853	3.027	511.1941	1547.384	104.8583	2
35	Copper	Potassium	0.101829818	0.333634338	3.268	522.2205	1706.617	102.6443	2
36	Copper	Sodium	0.109195287	0.333634338	3.047	619.4313	1887.407	86.53577	2
37	Copper	Magnesium	0.080730171	0.218677508	2.709	610.1577	1652.917	87.851	2
38	Copper	Titanium	0.111187483	0.218677508	1.967	481.0633	946.2516	111.426	2
39	Copper	Beryllium	0.100138722	0.218677508	2.184	738.7584	1613.448	72.55818	2
40	Caesium	Strontium	0.407034421	0.437355015	1.075	121.5347	130.6498	220.5254	1
41	Caesium	Calcium	0.565429651	0.437355015	0.774	154.9367	119.921	172.9834	1
42	Caesium	Praseodymium	11.9514404	0.665596064	0.074	97.88239	7.243297	273.8131	1
43	Caesium	Lithium	32.17862643	0.437355015	0.0141	191.6494	2.702257	139.8464	1
44	Erbium	Strontium	0.596957406	0.667268675	1.101	105.1533	115.7738	254.88	1
45	Erbium	Calcium	0.816947586	0.667268675	0.8	129.2647	103.4117	207.338	1

46	Erbium	Praseodymium	8.836976673	0.87471003	0.1	86.97044	8.697044	308.1677	1
47	Erbium	Lithium	11.73060336	0.667268675	0.0401	153.8538	6.169536	174.201	1
48	Erbium	Caesium	15.59668507	0.667268675	0.026	89.28904	2.321515	300.1654	1
49	Erbium	Calcium Hydroxide	34.14805932	0.665596064	0.02	238.9306	4.778612	224.3453	2
50	Barium Hydroxide	Strontium	0.441376896	0.497777238	1.111	206.9895	229.9653	258.9647	2
51	Barium Hydroxide	Calcium	0.602065359	0.497777238	0.81	253.5346	205.363	211.4227	2
52	Barium Hydroxide	Praseodymium	6.122688622	0.667268675	0.11	171.6655	18.88321	312.2524	2
53	Barium Hydroxide	Lithium	7.44253833	0.497777238	0.0501	300.6577	15.06295	178.2857	2
54	Barium Hydroxide	Caesium	9.430684871	0.497777238	0.036	176.1806	6.342502	304.2501	2
55	Barium Hydroxide	Erbium	74.28167688	0.667268675	0.01	158.3054	1.583054	338.6047	2
56	Barium Hydroxide	Calcium Hydroxide	14.82987903	0.437355015	0.03	234.6581	7.039744	228.43	2
57	Calcium Hydroxide	Strontium	0.453438761	0.497777238	1.081	331.4704	358.3195	161.7127	2
58	Calcium Hydroxide	Calcium	0.624733974	0.497777238	0.78	469.4985	366.2088	114.1707	2
59	Calcium Hydroxide	Praseodymium	8.448262128	0.667268675	0.08	249.3157	19.94525	215.0004	2
60	Calcium Hydroxide	Lithium	13.49621671	0.497777238	0.0201	661.4899	13.29595	81.03368	2
61	Calcium Hydroxide	Caesium	21.84889019	0.497777238	0.006	258.9539	1.553723	206.9981	2
62	Aluminium	Strontium	0.123417647	0.302417417	2.439	701.6	1711.202	114.6015	3
63	Aluminium	Calcium	0.140701279	0.302417417	2.138	1199.001	2563.464	67.05954	3
64	Aluminium	Praseodymium	0.357275329	0.511460433	1.438	478.9136	688.6778	167.8892	3
65	Aluminium	Lithium	0.217651357	0.302417417	1.3781	2370.237	3266.423	33.92254	3
66	Aluminium	Caesium	0.219882692	0.302417417	1.364	502.8831	685.9326	159.8869	3
67	Aluminium	Erbium	0.3841067	0.511460433	1.338	413.9405	553.8524	194.2415	3
68	Aluminium	Barium Hydroxide	0.249499492	0.32985498	1.328	886.8844	1177.782	181.3189	6
69	Aluminium	Calcium Hydroxide	0.243963534	0.32985498	1.358	1912.869	2597.675	84.06688	6
70	Aluminium	Lithiated Graphite	0.254269463	0.302417417	1.178	758.6145	893.6479	105.9885	3
71	Aluminium	Magnesium Hydroxide	0.322733308	0.32985498	1.028	2354.66	2420.591	68.29388	6
72	Aluminium	Potassium	0.236197548	0.302417417	1.269	1216.777	1544.09	66.07984	3
73	Aluminium	Sodium	0.285472352	0.302417417	1.048	1609.012	1686.245	49.97131	3
74	Aluminium	Magnesium	0.257351044	0.183417272	0.71	3135.499	2226.204	51.28654	6
75	Aluminium	Beryllium	0.977118744	0.183417272	0.185	4467.693	826.5232	35.99372	6
76	Lithiated Graphite	Strontium	0.346971815	0.437355015	1.261	160.8472	202.8283	166.627	1
77	Lithiated Graphite	Calcium	0.455819594	0.437355015	0.96	225.0618	216.0593	119.085	1
78	Lithiated Graphite	Praseodymium	2.753905314	0.665596064	0.26	121.8722	31.68676	219.9147	1
79	Lithiated Graphite	Lithium	2.191250974	0.437355015	0.2001	311.8337	62.39792	85.948	1
80	Lithiated Graphite	Caesium	2.357817327	0.437355015	0.186	126.4743	23.52423	211.9124	1
81	Lithiated Graphite	Erbium	4.697494998	0.665596064	0.16	108.831	17.41296	246.267	1
82	Lithiated Graphite	Barium Hydroxide	3.742674894	0.494782471	0.15	229.7161	34.45742	233.3443	2
83	Lithiated Graphite	Calcium Hydroxide	3.050442529	0.494782471	0.18	393.872	70.89696	136.0923	2

84	Lithiated Graphite	Potassium	4.833107344	0.437355015	0.091	226.9287	20.65051	118.1053	1
85	Magnesium Hydroxide	Strontium	0.348636546	0.497777238	1.411	367.2953	518.2537	145.9397	2
86	Magnesium Hydroxide	Calcium	0.44176861	0.497777238	1.11	544.7584	604.6818	98.39768	2
87	Magnesium Hydroxide	Praseodymium	1.631531762	0.667268675	0.41	269.0542	110.3122	199.2274	2
88	Magnesium Hydroxide	Lithium	1.356774809	0.497777238	0.3501	821.3669	287.5606	65.26068	2
89	Magnesium Hydroxide	Caesium	1.411002308	0.497777238	0.336	280.3135	94.18532	191.2251	2
90	Magnesium Hydroxide	Erbium	2.159564703	0.667268675	0.31	237.6232	73.66319	225.5797	2
91	Magnesium Hydroxide	Barium Hydroxide	1.460325421	0.437355015	0.3	252.063	75.61889	212.657	2
92	Magnesium Hydroxide	Calcium Hydroxide	1.327363673	0.437355015	0.33	464.4769	153.2774	115.405	2
93	Magnesium Hydroxide	Lithiated Graphite	2.984585128	0.497777238	0.15	390.3317	58.54976	137.3267	2
94	Magnesium Hydroxide	Potassium	1.930995336	0.497777238	0.241	550.2369	132.6071	97.41798	2
95	Magnesium Hydroxide	Sodium	13.53290844	0.497777238	0.02	659.2464	13.18493	81.30945	2
96	Potassium	Strontium	0.373970246	0.437355015	1.17	211.5044	247.4602	126.7183	1
97	Potassium	Calcium	0.50358009	0.437355015	0.869	338.5038	294.1598	79.1763	1
98	Potassium	Praseodymium	4.41693904	0.665596064	0.169	148.8922	25.16277	180.006	1
99	Potassium	Lithium	4.02752622	0.437355015	0.1091	582.1435	63.51186	46.0393	1
100	Potassium	Caesium	4.628512916	0.437355015	0.095	155.8192	14.80283	172.0037	1
101	Potassium	Erbium	13.13027636	0.665596064	0.069	129.8784	8.961608	206.3583	1
102	Potassium	Barium Hydroxide	12.0092171	0.494782471	0.059	277.1101	16.34949	193.4356	2
103	Potassium	Calcium Hydroxide	6.949169847	0.494782471	0.089	557.2981	49.59953	96.18364	2
104	Ferrate	Strontium	0.060593955	0.383674761	6.301	387.5574	2441.999	207.4646	3
105	Ferrate	Calcium	0.063618178	0.383674761	6	502.771	3016.626	159.9226	3
106	Ferrate	Praseodymium	0.109755167	0.58314002	5.3	308.3556	1634.285	260.7523	3
107	Ferrate	Zinc	0.08786361	0.262189643	2.9618	868.1363	2571.246	185.2346	6
108	Ferrate	Lithium	0.072789771	0.383674761	5.2401	634.1765	3323.148	126.7856	3
109	Ferrate	Copper	0.139074004	0.262189643	1.863	876.8655	1633.6	183.3906	6
110	Ferrate	Caesium	0.072985007	0.383674761	5.226	318.1185	1662.487	252.75	3
111	Ferrate	Erbium	0.11186054	0.58314002	5.2	280.0528	1456.275	287.1046	3
112	Ferrate	Barium Hydroxide	0.073421629	0.382057309	5.19	586.5043	3043.957	274.1819	6
113	Ferrate	Calcium Hydroxide	0.073000763	0.382057309	5.22	908.8845	4744.377	176.9299	6
114	Ferrate	Aluminium	0.057305241	0.222422892	3.862	547.6167	2114.896	146.8261	3
115	Ferrate	Lithiated Graphite	0.075662089	0.383674761	5.04	404.344	2037.894	198.8516	3
116	Ferrate	Magnesium Hydroxide	0.077913524	0.382057309	4.89	997.8403	4879.439	161.1569	6
117	Ferrate	Potassium	0.074328229	0.383674761	5.131	505.87	2595.619	158.9429	3
118	Ferrate	Cobalt	1.483444795	0.58314002	0.38	449.7451	170.9031	178.7778	3
119	Ferrate	Silver	1.989569686	0.58314002	0.28	353.0962	98.86692	227.7126	3
120	Ferrate	Sodium	0.077652835	0.383674761	4.91	562.9208	2763.941	142.8344	3
121	Ferrate	Magnesium	0.057069051	0.262189643	4.572	1115.569	5100.383	144.1496	6
122	Ferrate	Iron	0.404088837	0.58314002	1.43	457.6454	654.4329	175.6916	3
123	Ferrate	Iron Sulphate	0.18066436	0.262189643	1.429	670.5299	958.1872	239.8236	6
124	Ferrate	Titanium	0.068061382	0.262189643	3.83	958.7675	3672.079	167.7246	6
125	Ferrate	Beryllium	0.06443189	0.262189643	4.047	1247.966	5050.519	128.8568	6
126	Ferrate	Lithium Iron Phosphate	0.20955547	0.383674761	1.8	289.6372	521.347	277.604	3

127	Ferrate	Lithium Cobalt Oxide	0.354959156	0.383674761	1.05	369.3061	387.7714	217.7176	3
128	Cobalt	Strontium	0.112376742	0.667268675	5.921	182.8789	1082.826	146.5532	1
129	Cobalt	Calcium	0.118377576	0.667268675	5.62	270.6914	1521.286	99.0112	1
130	Cobalt	Praseodymium	0.177823351	0.87471003	4.92	134.1141	659.8413	199.8409	1
131	Cobalt	Zinc	0.212457598	0.550251816	2.5818	431.1582	1113.164	124.3232	2
132	Cobalt	Lithium	0.136822785	0.667268675	4.8601	406.8585	1977.373	65.8742	1
133	Cobalt	Copper	0.369014905	0.550251816	1.483	437.6495	649.0342	122.4792	2
134	Cobalt	Caesium	0.137219513	0.667268675	4.846	139.7085	677.0273	191.8386	1
135	Cobalt	Erbium	0.18151341	0.87471003	4.82	118.4893	571.1186	226.1932	1
136	Cobalt	Barium Hydroxide	0.138392191	0.665596064	4.81	251.3379	1208.935	213.2705	2
137	Cobalt	Calcium Hydroxide	0.137534298	0.665596064	4.84	462.0207	2236.18	116.0185	2
138	Cobalt	Aluminium	0.146827554	0.512025154	3.482	935.8632	3258.676	85.91474	3
139	Cobalt	Lithiated Graphite	0.14267686	0.667268675	4.66	194.2978	905.4279	137.9402	1
140	Cobalt	Magnesium Hydroxide	0.147598918	0.665596064	4.51	534.7167	2411.572	100.2455	2
141	Cobalt	Potassium	0.139953667	0.667268675	4.751	273.3966	1298.907	98.0315	1
142	Cobalt	Sodium	0.146756226	0.667268675	4.53	327.1547	1482.011	81.92297	1
143	Cobalt	Magnesium	0.131008061	0.550251816	4.192	643.9707	2699.525	83.2382	2
144	Cobalt	Iron	0.833864868	0.87471003	1.05	233.5027	245.1778	114.7802	1
145	Cobalt	Iron Sulphate	0.520511309	0.550251816	1.049	299.6048	314.2855	178.9122	2
146	Cobalt	Titanium	0.159117987	0.550251816	3.45	501.8384	1731.342	106.8132	2
147	Cobalt	Beryllium	0.1497228	0.550251816	3.667	788.9125	2892.942	67.94538	2
148	Cobalt	Lithium Iron Phosphate	0.464418637	0.667268675	1.42	123.6844	175.6318	216.6926	1
149	Cobalt	Lithium Cobalt Oxide	0.971586284	0.667268675	0.67	170.9211	114.5171	156.8062	1
150	Silver	Strontium	0.110515516	0.667268675	6.021	137.1004	825.4815	195.488	1
151	Silver	Calcium	0.116314092	0.667268675	5.72	181.1572	1036.219	147.946	1
152	Silver	Praseodymium	0.174280335	0.87471003	5.02	107.7335	540.8223	248.7757	1
153	Silver	Zinc	0.204559362	0.550251816	2.6818	309.3823	829.7015	173.258	2
154	Silver	Lithium	0.134073618	0.667268675	4.9601	233.4441	1157.906	114.809	1
155	Silver	Copper	0.345823007	0.550251816	1.583	312.7105	495.0208	171.414	2
156	Silver	Caesium	0.134454541	0.667268675	4.946	111.3141	550.5597	240.7734	1
157	Silver	Erbium	0.177823351	0.87471003	4.92	97.41459	479.2798	275.128	1
158	Silver	Barium Hydroxide	0.135573321	0.665596064	4.91	204.4312	1003.757	262.2053	2
159	Silver	Calcium Hydroxide	0.134749917	0.665596064	4.94	324.9583	1605.294	164.9533	2
160	Silver	Aluminium	0.14273452	0.512025154	3.582	596.253	2135.778	134.8495	3
161	Silver	Lithiated Graphite	0.139689978	0.667268675	4.76	143.4193	682.6759	186.875	1
162	Silver	Magnesium Hydroxide	0.144396853	0.665596064	4.61	359.3165	1656.449	149.1803	2
163	Silver	Potassium	0.137078566	0.667268675	4.851	182.3648	884.6517	146.9663	1
164	Silver	Cobalt	8.836976673	0.87471003	0.1	160.6792	16.06792	166.8012	1
165	Silver	Sodium	0.143597993	0.667268675	4.63	204.8138	948.288	130.8578	1
166	Silver	Magnesium	0.127961459	0.550251816	4.292	405.5515	1740.627	132.173	2
167	Silver	Iron	0.761290696	0.87471003	1.15	163.7082	188.2644	163.715	1
168	Silver	Iron Sulphate	0.475528627	0.550251816	1.149	235.2586	270.3121	227.847	2
169	Silver	Titanium	0.154646041	0.550251816	3.55	344.1647	1221.785	155.748	2
170	Silver	Beryllium	0.145756777	0.550251816	3.767	458.6146	1727.601	116.8802	2
171	Silver	Lithium Iron Phosphate	0.434198449	0.667268675	1.52	100.8988	153.3662	265.6274	1
172	Silver	Lithium Cobalt Oxide	0.848097772	0.667268675	0.77	130.2681	100.3064	205.741	1
173	Sodium	Strontium	0.314532683	0.437355015	1.391	242.3066	337.0485	110.6098	1
174	Sodium	Calcium	0.401430415	0.437355015	1.09	424.9632	463.2099	63.06777	1
175	Sodium	Praseodymium	1.790720803	0.665596064	0.39	163.5259	63.7751	163.8975	1

176	Sodium	Lithium	1.326960943	0.437355015	0.3301	895.4491	295.5878	29.93077	1
177	Sodium	Caesium	1.386265713	0.437355015	0.316	171.9199	54.32669	155.8952	1
178	Sodium	Erbium	2.449821094	0.665596064	0.29	140.8752	40.85382	190.2498	1
179	Sodium	Barium Hydroxide	1.887040588	0.494782471	0.28	302.283	84.63923	177.3271	2
180	Sodium	Calcium Hydroxide	1.693299405	0.494782471	0.31	669.4085	207.5166	80.07511	2
181	Sodium	Lithiated Graphite	3.37748113	0.437355015	0.13	262.7679	34.15983	101.9968	1
182	Sodium	Potassium	1.98354614	0.437355015	0.221	431.6688	95.3988	62.08807	1
183	Magnesium	Strontium	0.192031769	0.333634338	1.729	478.9186	828.0502	111.925	2
184	Magnesium	Calcium	0.232272587	0.333634338	1.428	832.5639	1188.901	64.383	2
185	Magnesium	Praseodymium	0.764560991	0.549407098	0.728	324.4482	236.1983	165.2127	2
186	Magnesium	Lithium	0.493183441	0.333634338	0.6681	1715.514	1146.135	31.246	2
187	Magnesium	Caesium	0.503681595	0.333634338	0.654	340.9632	222.9899	157.2104	2
188	Magnesium	Erbium	0.888158047	0.549407098	0.628	279.8161	175.7245	191.565	2
189	Magnesium	Barium Hydroxide	0.609237865	0.371086853	0.618	300.0574	185.4355	178.6423	2
190	Magnesium	Calcium Hydroxide	0.580639629	0.371086853	0.648	658.5912	426.7671	81.39034	2
191	Magnesium	Lithiated Graphite	0.700336664	0.333634338	0.468	518.8455	242.8197	103.312	2
192	Magnesium	Magnesium Hydroxide	1.200539362	0.371086853	0.318	816.9024	259.775	65.61734	2
193	Magnesium	Potassium	0.588014481	0.333634338	0.559	845.4286	472.5946	63.4033	2
194	Magnesium	Sodium	0.963171644	0.333634338	0.338	1133.38	383.0826	47.29477	2
195	Iron	Strontium	0.136517663	0.667268675	4.871	186.8129	909.9655	143.467	1
196	Iron	Calcium	0.145476408	0.667268675	4.57	279.4004	1276.86	95.925	1
197	Iron	Praseodymium	0.226082679	0.87471003	3.87	136.2177	527.1627	196.7547	1
198	Iron	Zinc	0.357320968	0.550251816	1.5318	442.1337	677.2604	121.237	2
199	Iron	Lithium	0.174363502	0.667268675	3.8101	426.8567	1626.367	62.788	1
200	Iron	Copper	1.247348763	0.550251816	0.433	448.9624	194.4007	119.393	2
201	Iron	Caesium	0.175008314	0.667268675	3.796	141.9928	539.0047	188.7524	1
202	Iron	Erbium	0.232081185	0.87471003	3.77	120.1284	452.884	223.107	1
203	Iron	Barium Hydroxide	0.177044174	0.665596064	3.76	255.0283	958.9065	210.1843	2
204	Iron	Calcium Hydroxide	0.175642581	0.665596064	3.79	474.6467	1798.911	112.9323	2
205	Iron	Aluminium	0.210082698	0.512025154	2.432	970.7336	2360.824	82.82854	3
206	Iron	Lithiated Graphite	0.183983637	0.667268675	3.61	198.7444	717.4674	134.854	1
207	Iron	Magnesium Hydroxide	0.192397082	0.665596064	3.46	551.7016	1908.888	97.15934	2
208	Iron	Potassium	0.179480277	0.667268675	3.701	282.2834	1044.731	94.9453	1
209	Iron	Sodium	0.190823602	0.667268675	3.48	339.9617	1183.067	78.83677	1
210	Iron	Magnesium	0.174675514	0.550251816	3.142	668.7664	2101.264	80.152	2
211	Iron	Titanium	0.228496881	0.550251816	2.4	516.7696	1240.247	103.727	2
212	Iron	Beryllium	0.209608792	0.550251816	2.617	826.4514	2162.823	64.85918	2
213	Iron	Lithium Iron Phosphate	1.72517704	0.667268675	0.37	125.4714	46.4244	213.6064	1
214	Iron Sulphate	Strontium	0.06836221	0.333634338	4.872	203.4685	991.2985	263.446	2
215	Iron Sulphate	Calcium	0.072855607	0.333634338	4.571	248.2722	1134.852	215.904	2
216	Iron Sulphate	Praseodymium	0.142274781	0.549407098	3.871	169.2367	655.1152	316.7337	2
217	Iron Sulphate	Zinc	0.142689058	0.218677508	1.5328	222.2198	340.6185	241.216	2
218	Iron Sulphate	Lithium	0.087350463	0.333634338	3.8111	293.2858	1117.741	182.767	2
219	Iron Sulphate	Copper	0.504160591	0.218677508	0.434	223.9316	97.18633	239.372	2
220	Iron Sulphate	Caesium	0.08767412	0.333634338	3.797	173.6233	659.2476	308.7314	2
221	Iron Sulphate	Erbium	0.146057084	0.549407098	3.771	156.2377	589.1723	343.086	2
222	Iron Sulphate	Barium Hydroxide	0.098901107	0.371086853	3.761	162.3529	610.6091	330.1633	2
223	Iron Sulphate	Calcium Hydroxide	0.098116613	0.371086853	3.791	230.1432	872.4729	232.9113	2

224	Iron Sulphate	Aluminium	0.075368708	0.183135699	2.433	792.9138	1929.159	202.8075	6
225	Iron Sulphate	Lithiated Graphite	0.09217968	0.333634338	3.611	210.3455	759.5574	254.833	2
226	Iron Sulphate	Magnesium Hydroxide	0.107495971	0.371086853	3.461	246.8609	854.3855	217.1383	2
227	Iron Sulphate	Potassium	0.089918907	0.333634338	3.702	249.4039	923.2933	214.9243	2
228	Iron Sulphate	Sodium	0.095613906	0.333634338	3.481	269.6112	938.5167	198.8158	2
229	Iron Sulphate	Magnesium	0.069581673	0.218677508	3.143	267.8394	841.8192	200.131	2
230	Iron Sulphate	Iron	-65.3401818	0.549407098	0.001	231.3734	0.231373	231.673	2
231	Iron Sulphate	Titanium	0.091087325	0.218677508	2.401	239.6134	575.3119	223.706	2
232	Iron Sulphate	Beryllium	0.083536573	0.218677508	2.618	289.9994	759.2184	184.8382	2
233	Iron Sulphate	Lithium Iron Phosphate	0.879393605	0.333634338	0.371	160.6874	59.61502	333.5854	2
234	Titanium	Strontium	0.134562999	0.333634338	2.471	395.5938	977.5123	135.5	2
235	Titanium	Calcium	0.153156289	0.333634338	2.17	609.4154	1322.431	87.958	2
236	Titanium	Praseodymium	0.376153815	0.549407098	1.47	283.9325	417.3808	188.7877	2
237	Titanium	Lithium	0.235203644	0.333634338	1.4101	977.7816	1378.77	54.821	2
238	Titanium	Caesium	0.237565074	0.333634338	1.396	296.5005	413.9147	180.7854	2
239	Titanium	Erbium	0.403800157	0.549407098	1.37	249.1539	341.3408	215.14	2
240	Titanium	Barium Hydroxide	0.274655334	0.371086853	1.36	265.076	360.5034	202.2173	2
241	Titanium	Calcium Hydroxide	0.268689322	0.371086853	1.39	510.673	709.8354	104.9653	2
242	Titanium	Aluminium	6.344809047	0.183135699	0.032	2148.084	68.73869	74.86154	6
243	Titanium	Lithiated Graphite	0.273831831	0.333634338	1.21	422.4465	511.1602	126.887	2
244	Titanium	Magnesium Hydroxide	0.353046154	0.371086853	1.06	600.9817	637.0406	89.19234	2
245	Titanium	Potassium	0.254801083	0.333634338	1.301	616.2797	801.7799	86.9783	2
246	Titanium	Sodium	0.306538943	0.333634338	1.08	756.3586	816.8673	70.86977	2
247	Titanium	Magnesium	0.294814647	0.218677508	0.742	742.5776	550.9926	72.185	2
248	Titanium	Beryllium	1.008912608	0.218677508	0.217	942.1851	204.4542	56.89218	2
249	Beryllium	Strontium	0.147469772	0.333634338	2.254	554.7113	1250.319	96.63218	2
250	Beryllium	Calcium	0.17010085	0.333634338	1.953	1091.928	2132.536	49.09018	2
251	Beryllium	Praseodymium	0.441790619	0.549407098	1.253	357.5441	448.0027	149.9199	2
252	Beryllium	Lithium	0.277683509	0.333634338	1.1931	3360.017	4008.837	15.95318	2
253	Beryllium	Caesium	0.280980937	0.333634338	1.179	377.7049	445.3141	141.9176	2
254	Beryllium	Erbium	0.480422472	0.549407098	1.153	304.092	350.6181	176.2722	2
255	Beryllium	Barium Hydroxide	0.327208197	0.371086853	1.143	328.1489	375.0742	163.3495	2
256	Beryllium	Calcium Hydroxide	0.318775721	0.371086853	1.173	810.9678	951.2653	66.09752	2
257	Beryllium	Lithiated Graphite	0.333170776	0.333634338	0.993	608.9918	604.7289	88.01918	2
258	Beryllium	Magnesium Hydroxide	0.44489486	0.371086853	0.843	1065.146	897.9181	50.32452	2
259	Beryllium	Potassium	0.305416492	0.333634338	1.084	1114.164	1207.754	48.11048	2
260	Beryllium	Sodium	0.382875424	0.333634338	0.863	1674.991	1445.517	32.00195	2
261	Beryllium	Magnesium	0.416730412	0.218677508	0.525	1608.869	844.656	33.31718	2
262	Lithium Iron Phosphate	Strontium	0.09717939	0.437355015	4.501	109.2247	491.6203	245.3794	1
263	Lithium Iron Phosphate	Calcium	0.104144756	0.437355015	4.2	135.4723	568.9836	197.8374	1
264	Lithium Iron Phosphate	Praseodymium	0.191170305	0.665596064	3.5	89.73698	314.0794	298.6671	1
265	Lithium Iron Phosphate	Zinc	0.288725311	0.332798032	1.1618	240.2111	279.0773	223.1494	2
266	Lithium Iron Phosphate	Lithium	0.127153186	0.437355015	3.4401	162.7287	559.8031	164.7004	1
267	Lithium Iron Phosphate	Copper	6.180569609	0.332798032	0.063	242.2127	15.2594	221.3054	2
268	Lithium Iron Phosphate	Caesium	0.127676574	0.437355015	3.426	92.20754	315.903	290.6648	1

269	Lithium Iron Phosphate	Erbium	0.196823402	0.665596064	3.4	82.46118	280.368	325.0194	1
270	Lithium Iron Phosphate	Barium Hydroxide	0.14672393	0.494782471	3.39	171.7511	582.2364	312.0967	2
271	Lithium Iron Phosphate	Calcium Hydroxide	0.145430145	0.494782471	3.42	249.4963	853.2774	214.8447	2
272	Lithium Iron Phosphate	Aluminium	0.146989567	0.301323318	2.062	435.2282	897.4405	184.7409	3
273	Lithium Iron Phosphate	Lithiated Graphite	0.135007305	0.437355015	3.24	113.198	366.7616	236.7664	1
274	Lithium Iron Phosphate	Magnesium Hydroxide	0.161051505	0.494782471	3.09	269.2646	832.0276	199.0717	2
275	Lithium Iron Phosphate	Potassium	0.131318461	0.437355015	3.331	136.1465	453.504	196.8577	1
276	Lithium Iron Phosphate	Sodium	0.140651621	0.437355015	3.11	148.28	461.1508	180.7491	1
277	Lithium Iron Phosphate	Magnesium	0.120454796	0.332798032	2.772	294.4177	816.1258	182.0644	2
278	Lithium Iron Phosphate	Titanium	0.164682542	0.332798032	2.03	260.6649	529.1497	205.6394	2
279	Lithium Iron Phosphate	Beryllium	0.148713564	0.332798032	2.247	321.4155	722.2207	166.7715	2
280	Lithium Cobalt Oxide	Strontium	0.083297919	0.437355015	5.251	144.4878	758.7056	185.493	1
281	Lithium Cobalt Oxide	Calcium	0.088363626	0.437355015	4.95	194.2826	961.699	137.951	1
282	Lithium Cobalt Oxide	Praseodymium	0.157288411	0.665596064	4.25	112.2431	477.0331	238.7807	1
283	Lithium Cobalt Oxide	Zinc	0.174913283	0.332798032	1.9118	328.3228	627.6875	163.263	2
284	Lithium Cobalt Oxide	Lithium	0.10439085	0.437355015	4.1901	255.7052	1071.43	104.814	1
285	Lithium Cobalt Oxide	Copper	0.414007277	0.332798032	0.813	332.0734	269.9757	161.419	2
286	Lithium Cobalt Oxide	Caesium	0.104743362	0.437355015	4.176	116.1351	484.9803	230.7784	1
287	Lithium Cobalt Oxide	Erbium	0.161095288	0.665596064	4.15	101.0869	419.5108	265.133	1
288	Lithium Cobalt Oxide	Barium Hydroxide	0.120028733	0.494782471	4.14	212.5328	879.8857	252.2103	2
289	Lithium Cobalt Oxide	Calcium Hydroxide	0.119161515	0.494782471	4.17	345.9185	1442.48	154.9583	2
290	Lithium Cobalt Oxide	Aluminium	0.107616855	0.301323318	2.812	643.9849	1810.886	124.8545	3
291	Lithium Cobalt Oxide	Lithiated Graphite	0.109626758	0.437355015	3.99	151.5235	604.5789	176.88	1
292	Lithium Cobalt Oxide	Magnesium Hydroxide	0.129449647	0.494782471	3.84	385.1193	1478.858	139.1853	2
293	Lithium Cobalt Oxide	Potassium	0.107181946	0.437355015	4.081	195.6722	798.5384	136.9713	1
294	Lithium Cobalt Oxide	Sodium	0.113319337	0.437355015	3.86	221.7513	855.9602	120.8628	1
295	Lithium Cobalt Oxide	Magnesium	0.094737443	0.332798032	3.522	438.7284	1545.202	122.178	2
296	Lithium Cobalt Oxide	Iron	1.840230393	0.665596064	0.38	174.3526	66.25399	153.72	1
297	Lithium Cobalt Oxide	Iron Sulphate	0.899829026	0.332798032	0.379	246.0522	93.25378	217.852	2
298	Lithium Cobalt Oxide	Titanium	0.120107018	0.332798032	2.78	367.7658	1022.389	145.753	2
299	Lithium Cobalt Oxide	Beryllium	0.111383936	0.332798032	2.997	501.5004	1502.997	106.8852	2
300	Lithium Cobalt Oxide	Lithium Iron Phosphate	0.583535676	0.437355015	0.75	104.8439	78.63289	255.6324	1